JREE: Vol. 11, No. 2, (Spring 2024) 30-46

Journal of Renewable Energy and Environment

Journal Homepage: www.jree.ir

Materials and Energy Research Center

MERC

Research Article

Enhanced LVRT and HVRT Capability of Grid Tied PMSG Based Wind Energy System Using Active Disturbance Rejection Controller

Sagiraju Dileep Kumar Varma*, Sarathbabu Sri Satya Sita Duvvuri, Omkar Koduri, Srikanth Venkata Malladi

Department of Electrical & Electronics Engineering, Shri Vishnu Engineering College for Women Bhimavaram (Autonomous), Andhra Pradesh, India.

PAPER INFO

Paper history:
Received: 01 August 2023
Revised: 05 December 2023
Accepted: 03 January 2024

Keywords:
Active Disturbance Rejection Controller,
Proportional Resonant Controller,
Harmonic Compensator,
Fault Ride Through Capability,
Proportional Integral Controller,
Permanent Magnet Synchronous Generator

ABSTRACT

The widespread integration of wind energy poses numerous challenges, including ride-through capability issues, stability concerns, and power quality issues within the utility grid. Additionally, the inherent non-linear nature of wind energy systems, coupled with internal dynamics like model uncertainties, non-linearities, parametric variations, modeling errors, and external disturbances, significantly impacts system performance. Therefore, developing a robust controller becomes imperative to address the complexity, non-linearity, coupling, time variation, and uncertainties associated with wind energy systems, aiming to enhance transient performance in the presence of external and internal disturbances. The research presented in this manuscript focuses on devising a robust control scheme for a grid-tied Permanent Magnet Synchronous Generator (PMSG) wind turbine. The objective is to improve the wind turbine's performance under both normal and abnormal grid conditions. The innovation in Active Disturbance Rejection Control (ADRC) lies in its capacity to offer robust, adaptive, and disturbance-rejecting capabilities without relying on precise mathematical models. This quality makes ADRC a valuable and innovative tool for addressing challenges in complex and dynamic real-world applications where system parameters evolve over time. The wind energy system is inherently non-linear, time-varying, cross-coupled, and highly uncertain. It is also susceptible to parameter uncertainties, parametric variations, and external grid disturbances, all of which significantly influence its performance. The effectiveness of the proposed control scheme is validated to enhance ride-through capability and extract maximum power under internal disturbances, external grid disturbances, and parametric variations. To assess the proposed controller's efficacy, a comparative analysis is conducted using the Integral Time Absolute Error (ITAE) index for all abnormal grid disturbances. This analysis is performed in comparison to a Proportional Resonant Controller and a PI controller, providing evidence of the proposed controller's effectiveness. In summary, the incorporation of an Active Disturbance Rejection Controller emerges as a promising solution for enhancing the Low Voltage Ride-Through (LVRT) and High Voltage Ride-Through (HVRT) capabilities of grid-tied Permanent Magnet Synchronous Generator (PMSG)-based wind energy systems.

https://doi.org/10.30501/jree.2024.409369.1642

1. INTRODUCTION

Conventional energy sources have a detrimental effect on the environment, primarily due to carbon emissions. In response to these challenges, there has been a notable shift towards exploring alternative energy resources. Solar, wind, and hydro energy sources are garnering significant interest, driven by the depletion of fossil fuels, growing environmental concerns, and the threat of global warming. Among these alternatives, wind energy systems have gained widespread recognition as a superior technology, offering advantages over other energy sources.

A. Research background and Motivation

The wind energy system is exposed to both external and internal disturbances. External grid faults, including symmetrical faults, asymmetrical faults, and voltage surges due to sudden load loss, can lead to the tripping of wind turbines. However, the sudden disconnection of wind turbines from the grid is not allowed according to the modern grid codes established by each country. In addition to external perturbations, internal disturbances such as model uncertainties, modeling errors, unmodeled dynamics, grid parametric variations, and non-linearities result in significant variations in machine and grid parameters.

B. Literature Review and Limitations

The wind energy system is exposed to both external and internal disturbances. External grid faults, including symmetrical faults, asymmetrical faults, and voltage surges due to sudden load loss, can lead to the tripping of wind turbines. However, the sudden disconnection of wind turbines from the grid is not allowed according to the modern grid codes established by each country. In addition to external perturbations, internal disturbances such as model uncertainties, modeling errors, unmodeled dynamics, grid parametric variations, and non-linearities result in significant variations in machine and grid parameters. Fault ride-through

*Corresponding Author's Email: *varma8332@gmail.com* (S. D. K. Varma)
URL: https://www.jree.ir/article_187157.html

Please cite this article as: Varma, S. D. K., Duvvuri, S. S. S. S., Koduri, O. & Malladi, S. V. (2024). Enhanced LVRT and HVRT Capability of Grid Tied PMSG Based Wind Energy System Using Active Disturbance Rejection Controller, *Journal of Renewable Energy and Environment (JREE)*, 11(2), 30-46. https://doi.org/10.30501/jree.2024.409369.1642.

(FRT) improvement solutions are depicted in Figure 1. The first category of low-voltage ride-through (LVRT) capability enhancement schemes relies on external hardware-based solutions, including battery energy storage devices, Braking Chopper (BC), Flexible Alternating Current Transmission Systems (FACTS) devices, pitch angle controller-based methods, and series Dynamic Breaking Resistor (DBR) (Hosseini, Behzadfar, Hashemi, Moazzami, & Dehghani, 2022). Various energy storage devices have been reported in the literature to mitigate power fluctuations. For instance, the use of a battery energy storage system to enhance the LVRT of a grid-tied Permanent Magnet Synchronous Generator (PMSG) wind turbine is detailed in (Lu, M. S., et., 2009) The advantage of integrating a battery energy storage system at the dc-link interface lies in its ability to enhance LVRT by absorbing surplus energy accumulated in the dc-link capacitor. However, larger-rated battery energy storage devices are required to handle power variations between the generator and the grid during grid disturbances. References (Bolund, Bernhoff, & Leijon, 2007) and (Díaz-González, Sumper, Gomis-Bellmunt, & Bianchi, 2013) proposed Flywheel Energy Storage System (FESS) as an alternative energy storage method to stabilize power variations in integrated wind power systems. Nevertheless, this method may not be suitable for large-sized wind turbines due to increased system costs. In (Abbey & Joos, 2007) and (Rahim & Nowicki, 2012), a supercapacitor-based energy storage device was presented to augment LVRT capability. Supercapacitors store additional energy at the DC-link during fault conditions, limiting the generator speed and preventing wind farm detachment. However, proper sizing of the storage device is essential to consume energy produced under the most severe fault conditions. References (Shi, Tang, Xia, Ren, & Li, 2011) and (Nguyen T.H & Lee, 2010) discussed the implementation of a Superconducting Magnetic Energy Storage (SMES) device to enhance Fault Ride Through (FRT) capability and smooth PMSG output capacity. Despite having unlimited charging and discharging cycles compared to other storage systems, the use of SMES increases the overall system cost when integrating large wind farms into the grid system. LVRT capability improvement by storing energy in the turbine generator inertia under grid faults was explored in (Alepuz, Calle, Busquets-Monge, Kouro, & Wu, 2013) and (Guoyi, X., Lie, X., & Morrow, J. 2013) In this method, the power disparity between generated power and grid power is accumulated in the dc-link during grid faults, stored in rotor inertia by accelerating the rotor to its upper limit. However, this method is only applicable when grid faults persist for a short period. Another LVRT method for boosting Point of Common Coupling (PCC) voltage during fault conditions is the series dynamic braking resistor, presented in (Causebrook, Atkinson, & Jack, 2007). This approach is relatively easy and less costly to enhance ride-through capability. However, fault currents increase losses in the braking resistor since it is a series device connected between the wind turbine and the grid. In (Pannell, Zahawi, Atkinson, & Missailidis, 2013), a braking chopper was discussed to boost LVRT capability. While a relatively simple and low-cost device, the required reactive power cannot be pumped into the grid as specified by grid codes, necessitating the dissipation of all power to relax the grid-side converter capacity during faults. References in (Mohod & Aware, 2010; Wang, L., & Truong, D. N. 2012; T. H. Nguyen & Lee, 2013) discussed FACT devices based on shunt compensation for grid-connected PMSG to enhance LVRT capability. This scheme provides voltage support at PCC by regulating reactive power but cannot offer real power support during grid interruptions. The authors in (Ramirez, Martinez, Platero, Blazquez, & Castro, 2011;Chen, Yan, Zhou, & Sun, 2018) implemented a series compensation-based device, called Dynamic Voltage Restorer (DVR), to enhance LVRT requirements. This device can deliver and absorb both real and reactive power. Unified Power Flow Controller (UPFC), discussed in (Golshannavaz, Aminifar, & Nazarpour, 2014; Raphael & Massoud, 2011), is considered the most effective hybrid compensation-based FACTS device for LVRT applications, combining series and shunt compensation features. However, the key drawback is the increased overall system cost. In (Thet & Saitoh, 2009), a pitch angle-based controller was proposed to improve the LVRT requirement of the PMSG wind turbine system. By regulating the pitch angle, mechanical input power to the wind turbine can be limited, offering a relatively simple and cost-effective solution. Nevertheless, the mechanical system's response may not be fast enough to voltage dips caused by symmetrical and asymmetrical faults. Superconducting fault current limiter, discussed in (Huang, Xiao, Zheng, & Wang, 2019; Yehia, Mansour, & Yuan, 2018), is another option to recover LVRT capability for PMSG wind turbines by limiting fault current. This scheme is relatively better than hardware-based LVRT solutions, offering medium cost, less complexity, and better dc voltage protection under fault conditions. However, it requires a higher cost for superconducting material and a cooling system.

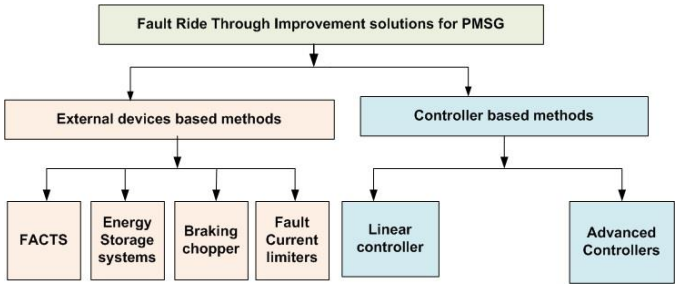

Figure 1. Fault ride-through improvement solutions of the PMSG

To overcome the limitations of superconducting fault current limiters, a Bridge-type Fault Current Limiter (BFCL) was suggested in (Firouzi, M. 2018; Alam, S., & Abido, M. 2018). It provides dynamic resistance control for a wide range of voltage sags, proving to be effective compared to superconducting fault current limiters. However, turning on Insulated Gate Bipolar Transistors (IGBTs) in BFCL leads to high transient overvoltage, potentially causing mal operation. In (Ji, He, Li, Liu, & Zhang, 2014), a Series Dynamic Braking Resistor (SDBR) was proposed to enhance LVRT in wind energy systems. Under fault conditions, the current flowing through SDBR increases voltage drop, preventing overvoltage at the dc link. However, the scheme is more susceptible to switching delay and underperforms in terms of enhancing transient stability in low-voltage grid conditions.

C. Research Gaps

The wind energy system is highly nonlinear, time-varying, cross-coupled, and inherently uncertain. It is also subject to parameter uncertainties and external disturbances, which significantly impact the system's performance. According to published literature, there is a noticeable increase in cost when employing external device-based solutions to enhance the Low Voltage Ride Through (LVRT) of a Permanent Magnet Synchronous Generator (PMSG)-based wind turbine.

Therefore, to enhance fault ride-through capability, controller-based techniques have been proposed as alternatives to external device-based solutions. The majority of these controller-based approaches are model-dependent. Various control schemes for wind turbine systems are recommended in the literature, such as vector control techniques, direct control schemes, hysteresis control schemes, and advanced control schemes, all aimed at improving the dynamic performance of PMSG-based wind energy systems. While existing control schemes perform satisfactorily under linear operating conditions, they struggle in wide operating regions. Furthermore, these schemes do not account for internal parametric variations and uncertainties. Additionally, the complexity of controllers increases due to reference frame transformations, cross-coupled terms, chattering, noise, harmonic rejection, and changing switching frequency. The performance of these control methods is unsatisfactory in the presence of a highly nonlinear, time-varying, cross-coupled, and uncertain wind energy system, along with parametric fluctuations and model uncertainties. In (Inoue, Y., Morimoto, S., & Sanada, M. 2008; Kwon, J. et., 2008) the authors described the application of the Vector PI controller and direct torque control for the PMSG wind turbine system. The mathematical framework of these control techniques relies on precise system parameter information. Additionally, the performance of the control scheme is susceptible to both internal and external disruptions, which significantly degrade the controller's performance. To overcome these limitations, advanced nonlinear control schemes are discussed in (Soliman, M. et., 2019; Muyeen, S. M., & Al-Durra, A. 2013) subsequently. Soft computing techniques, such as fuzzy logic and ANN-based control methods, offer distinct advantages over conventional controllers. The fuzzy logic controller is model-independent and insensitive to variations in system parameters, making it suitable for implementation in complex nonlinear systems. However, the type-1 fuzzy control scheme does not address uncertainties in complex systems. To overcome these shortcomings, researchers have focused on nonlinear control schemes. The feedback linearization technique, proposed in (Cheikh, R et., 2020; Kim, K et.al 2012). aims to enhance the Low Voltage Ride Through (LVRT) capability of the PMSG wind turbine system. The feedback linearization scheme is implemented for the Machine-Side Converter (MSC) of PMSG to control the DC link voltage of the full-scale converter. However, this method falls short in providing sufficient reactive power support during fault ride-through operations. To address this limitation, a backstepping nonlinear scheme for both the machine-side converter and grid-side converter of the PMSG was employed in (Ayadi, M., & Derbel, N. 2017) to improve the ride-through capability of the PMSG wind energy system. The authors in (Valenciaga, F., & Puleston, P. F. 2008; Merabet, A et.al 2016) described sliding mode control for grid tied PMSG wind energy to enhance LVRT capability in internal and external perturbations. It is one of the most adaptive non-linear control schemes and is insensitive to varying uncertainties and parameter variations. Model Predictive Control (MPC) is applied for grid tied wind energy system in (Yaramasu, V. et al., 2014) However, MPC also suffers from some limitations particularly in wind energy conversion system with severe internal and external perturbations and uncertainties of wind speed variation. The performance of these control schemes is not adequate in the occurrence of model uncertainties, parametric variations and internal unknown dynamics. In view of this, an Active disturbance rejection controller has been developed to deal with the rejection of unknown internal and external perturbations for grid-tied wind energy systems to improve fault ride through enhancement. Since ADRC is not dependent on the mathematical model, it is not affected by lumped disturbances or parametric changes. Additionally, ADRC requires less tuning parameters. Hence, ADRC is widely recognized in a variety of engineering challenges, such as the wind energy system. This control scheme has been applied in (Laghridat, H., et., 2022; Penne, M., et., 2021; Belachew Desalegn et., 2023; Elmouhi, Noureddine et., 2023; Liu, M. et al., 2023; Wang, Z., 2023) SCIG and DFIG Wind farms to address the issue of fault ride-through capability However, ride through capability on utility side disturbances such as distorted grid conditions, low and high voltage conditions as well as source side disturbances such as variable speed conditions has not been applied on PMSG based wind turbines. Hence, this manuscript investigates LVRT and HVRT capability on PMSG-based wind turbine using an Active Disturbance Rejection Controller.

D. Research Contribution

The primary objective of this study is to develop a robust controller that can adapt to external disturbances, internal disturbances and environmental conditions. Hence, this paper recommends an Active Disturbance Rejection Controller (ADRC) for enhancing the performance of a PMSG wind turbine in abnormal grid conditions.

The key objectives of this paper are summarized below:

- To establish the mathematical framework of ADRC is established for the grid side inverter to expand the performance of a grid tied PMSG wind turbine in external disturbances such as symmetrical fault, asymmetrical fault conditions, voltage swell conditions, distorted grid conditions, and variable speed conditions
- To develop a mathematical framework of ADRC for the machine side converter to enrich the performance of the grid-tied PMSG wind turbine in external time varying wind variations.
- To recover the LVRT and HVRT capability of the grid tied wind turbine under symmetric and asymmetric fault conditions.
- To inspect the performance of PMSG wind energy under distorted grid conditions and machine parametric variations to enhance power quality.

E. Organization of Paper

This study is structured as in the following manner. Section 1 discusses the introduction part. Section 2 presents the test system. Section 3 introduces the proposed control scheme. Section 4 explores the results and discussion elaborately. Lastly, Section 5 stretches conclusions.

2. TEST SYSTEM

The PMSG wind turbine is coupled to an external grid with the help of fully rated power electronic converters, as displayed in Fig. 2. The machine and the utility side inverter are separated by a dc-link capacitor. The objective of the source side converter is utilized to take available peak power from wind. In contrast, the grid side inverter is used to control dc link voltage and reactive power.

2.1. Fundamental Proportional Resonant Control Scheme

The PR controller is depicted in Fig 3(a). The PR control method provides a high gain at the resonant frequency, ensuring minimal steady-state error between the measured and reference signals. The proposed system is designed and tuned at the resonant frequency in a single stationary reference frame to regulate both positive and negative sequence components simultaneously. As a result, the complexity is reduced with the proposed controller. The transfer function of proportional resonant control is as follows:

$$H_{ab}(s) = k_p + \frac{k_{ri}s}{s^2 + \omega_r^2} \quad (1)$$

where k_p signifies proportional gain, k_{ri} symbolizes the resonant gain, and ω_r is resonant frequency.

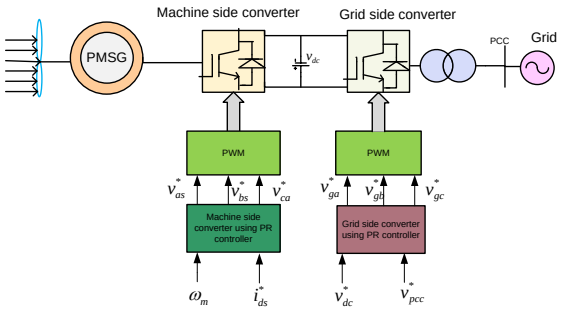

Figure 2. Block diagram of test system

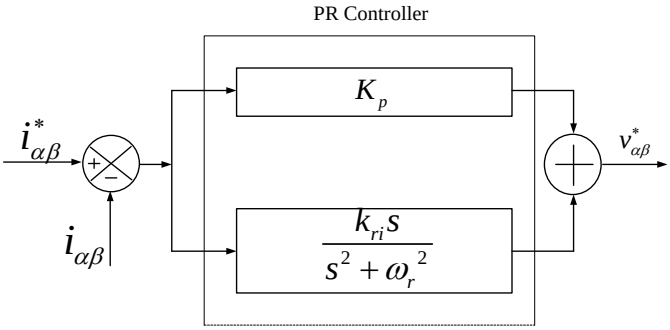

Figure 3 (a). Schematic diagram of resonant controller

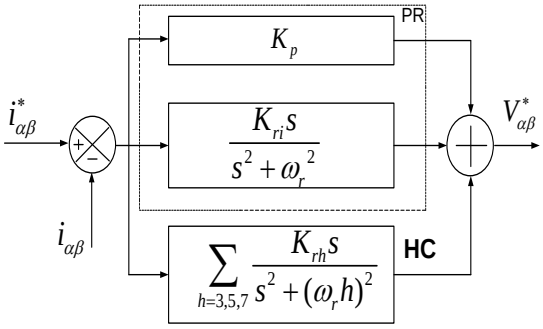

Figure 3 (b). PR Controller with harmonic compensator

2.2. Fundamental Proportional Resonant with Harmonic Compensator

In Fig. 3(b), the PR controller, in conjunction with the harmonic compensator, is depicted, aiming to enhance the quality of the injected grid current. The Harmonic Compensator (HC) is intended to mitigate harmonics in the grid current. It is designed with a resonant frequency set to the specific frequency requiring compensation. To suppress lower-order harmonics, a dedicated harmonic compensator is designed in tandem with the PR controller:

The transfer function of HC is specified by:

$$G_{HC}^{h}(s) = \frac{k_{rh}s}{s^2 + (\omega_r h)^2} \quad (2)$$

where k_{rh} is the resonant gain at the particular harmonic, h is the order of harmonic, and $\omega_r h$ is the resonant frequency of the specific harmonic.

3. THE PROPOSED ACTIVE DISTURBANCE REJECTION CONTROL SCHEME

This section introduces the proposed scheme for a grid-interfaced PMSG wind turbine system. Firstly, we delve into the basic mathematical framework of Active Disturbance Rejection Control. Following that, we develop the mathematical framework of the proposed approach for MSC and GSC.

This study is structured as in the following manner. Section 1 discusses the introduction part. Section 2 presents the test system. Section 3 introduces the proposed control scheme. Section 4 explores the results and discussion elaborately. Lastly, Section 5 stretches conclusions.

3.1. Basic ADRC Control Scheme

Fig. 4(a) illustrates the schematic representation of ADRC. ADRC essentially comprises a feedback control system with a proportional controller and a perturbation elimination loop incorporating an Extended State Observer (ESO). The ESO actively predicts the system's state variables and lumped perturbation, encompassing both internal and external perturbations. Subsequently, the control law is applied to reject both internal and external disruptions. One of the key advantages of ADRC is model independence, wherein the tuning process focuses solely on the observer bandwidth and controller gain parameters. The foundational mathematical framework of ADRC is provided here.

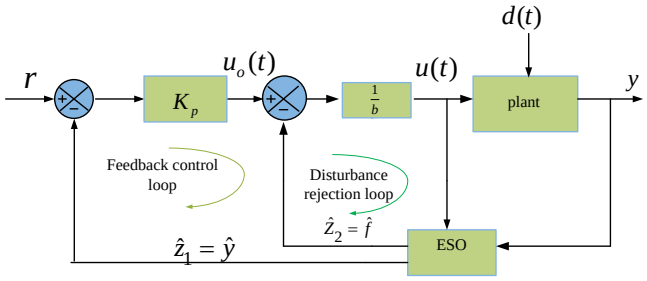

Figure 4 (a). Schematic diagram of ADRC control scheme

The flowchart of the proposed method is shown in Figure 4(b).

Step 1: System modeling: Mathematical model of the system is developed, which is to be controlled;

Step 2: The developed model is converted into state space representation as a first-order differential equation;

Step 3: Extended State Observer (ESO) has been designed to estimate lumped disturbance including internal and external disturbances;

Step 4: Controller design: Formulated based on the control law, which is developed in accordance with the estimated state and disturbance information acquired from the Extended State Observer (ESO);

Step 5: The tuning of ADRC is achieved by adjusting observer gains and gain of the controller.

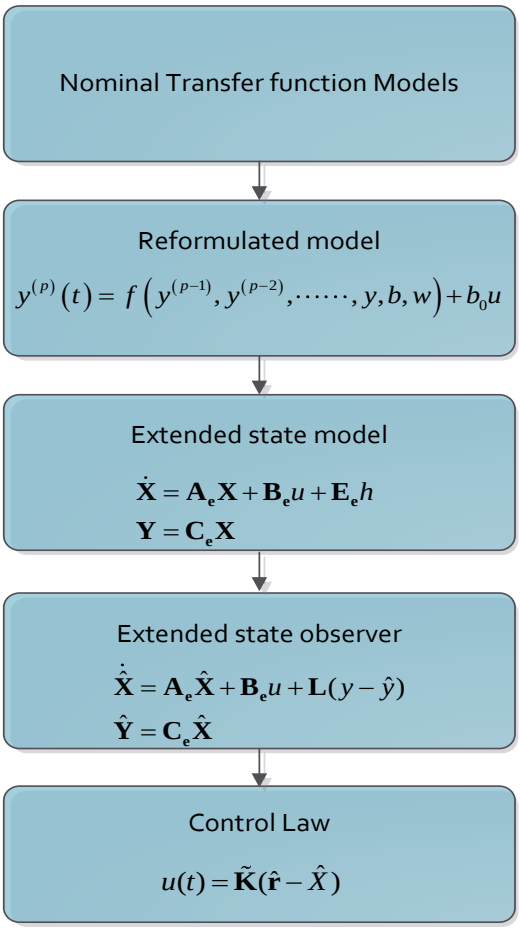

Figure 4 (b). Flowchart of the proposed controller

3.2. Basic ADRC Control Scheme

The proposed ADRC for the source side converter is presented in Fig. 5. In order to maximize power extraction, MSC is controlled to modify the speed of the rotor and torque with respect to variations in wind velocity. Two internal current loops and an external OTC-MPPT control are included in this control strategy. The abc/dq transformation is used to translate the three phase stator currents into the dq components. The optimal torque control approach is used to determine reference quadrature stator current. With the suggested ADRC approach, the real stator currents in dq axes are precisely following their reference. The reference dq is produced by the ADRC.

The Electromagnetic torque is given by:

$$T_e = \frac{3}{2} p\phi_m i_{qs} \tag{3}$$

Stator refwerence q-axis current from (3) is given by

$$i_{qs}^* = \left(\frac{2}{3p\phi_m}\right) T_e^* \tag{4}$$

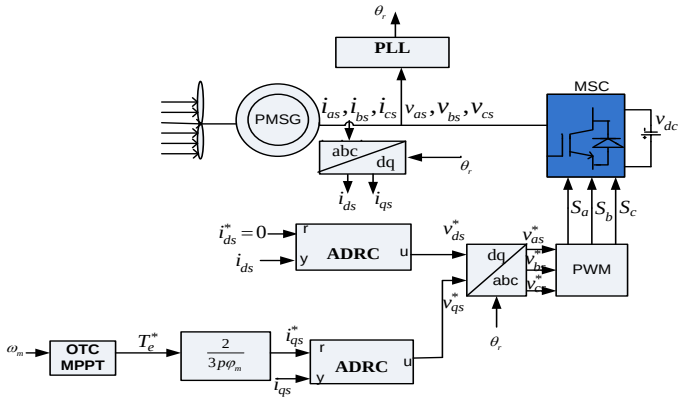

Figure 5. Proposed ADRC for machine side converter

3.3. Mathematical Model of ADRC for a Source Side Converter

This section provides an overview of theoretical framework of ADRC for the PMSG MSC side of the wind turbine. The voltage in dq-axes with flux orientation is specified by:

$$v_{ds} = i_{ds}R_s + L_s\frac{di_{ds}}{dt} - \omega_e L_{qs} i_{qs}$$

$$v_{qs} = i_{qs}R_s + L_s\frac{di_{qs}}{dt} + \omega_e L_{ds} i_{ds} + \omega_e \psi_m \tag{5}$$

Equation (5) is specified as

$$L_{ds}\frac{di_{ds}}{dt} = v_{ds} - i_{ds}R_s + \omega_e L_{qs} i_{qs}$$

$$L_{qs}\frac{di_{qs}}{dt} = v_{qs} - i_{qs}R_s - \omega_e L_{ds} i_{ds} - \omega_e \psi_m \tag{6}$$

The cononical form of equation (6) is:

$$\dot{i}_{ds} = \left(-\frac{R_s}{L_{ds}} i_{ds} + \omega_e i_{qs}\frac{L_{qs}}{L_{ds}}\right) + \frac{v_{ds}}{L_{ds}}$$

$$\dot{i}_{qs} = \left(-\frac{R_s}{L_{qs}} i_{qs} - \frac{1}{L_{qs}}\left(\omega_e L_{ds} i_{ds} + \omega_e \psi_m\right)\right) + \frac{v_{qs}}{L_{qs}} \tag{7}$$

where $f_d\left(i_{ds}, t\right)$ and $f_q\left(i_{qs}, t\right)$ denote internal disturbance in *dq*-axes

$$f_d\left(i_{ds}, t\right) = \left(-\frac{R_s}{L_{ds}} i_{ds} + \omega_e i_{qs}\frac{L_{qs}}{L_{ds}}\right);$$

$$f_q\left(i_{qs}, t\right) = \left(-\frac{R_s}{L_{qs}} i_{qs} - \frac{1}{L_{qs}}\left(\omega_e L_{ds} i_{ds} + \omega_e \psi_m\right)\right)$$

By taking external perturbastion $d(t)$ into account, equation (15) is re-written as:

$$\dot{i}_{ds} = f_d(i_{ds}, t) + d(t) + bu_d(t)$$

$$\dot{i}_{qs} = f_q(i_{qs}, t) + d(t) + bu_q(t) \tag{8}$$

$u_d(t)$ and $u_d(t)$ represent the control signals

$$u_d(t) = v_{ds}; u_q(t) = v_{qs}; b_0 = \frac{1}{L_s}$$

The total perturbation including internal and external disturbance is characterized by $f_{ds}(t)$ and $f_{qs}(t)$

$$f_{ds}(t) = f_d(i_{ds}, t) + d(t)$$

$$f_{qs}(t) = f_q(i_{qs}, t) + d(t) \tag{9}$$

Thus, the stator current in qd-axes is given by:

$$\dot{i}_{ds} = f_{ds}(t) + b_o u_d(t)$$
$$\dot{i}_{qs} = f_{qs}(t) + b_o u_q(t) \quad (10)$$

3.4. Mathematical Model of the proposed ADRC for *dq* current control

The mathematical model of ADRC for inner qd-axes current control is given here:

STEP 1: Canonical form of ADRC for direct axis stator current loop is:

Equation (10) is written by

$$\dot{i}_{ds} = f_{ds}(t) + bu_d(t) \quad (11)$$

Let

$$x_1 = y = i_{ds}; x_2 = f_{ds}(t)$$

STEP 2: The state space model is formulated as follows: The state space model of equation (11) is:

$$\dot{x}_1 = x_2 + bu_d(t)$$
$$\dot{x}_2 = \dot{f}_{ds}(t) \quad (12)$$
$$y = x_1$$

The matrix representation of equation (12) is

$$\begin{pmatrix}\dot{x}_1\\ \dot{x}_2\end{pmatrix} = \begin{pmatrix}0 & 1\\ 0 & 0\end{pmatrix}\begin{pmatrix}x_1\\ x_2\end{pmatrix} + \begin{pmatrix}b\\ 0\end{pmatrix}u_d(t) + \begin{pmatrix}0\\ 1\end{pmatrix}\dot{f}_{ds}$$
$$y = \begin{pmatrix}1 & 0\end{pmatrix}\begin{pmatrix}x_1\\ x_2\end{pmatrix} \quad (13)$$

Equation (13) is given by:

$$\dot{\mathrm{x}} = \mathbf{A}\mathrm{x} + \mathbf{B}\mathrm{u}_d(t)$$
$$\mathrm{y} = \mathbf{C}\mathrm{x} \quad (14)$$

Where

$$\mathrm{A} = \begin{pmatrix}0 & 1\\ 0 & 0\end{pmatrix}; \mathrm{B} = \begin{pmatrix}1\\ 0\end{pmatrix}; \mathrm{C} = \begin{bmatrix}1 & 0\end{bmatrix}; E = \begin{pmatrix}0\\ 1\end{pmatrix}$$

STEP 3: Formulation of Extended State Observer

Then, the ESO model is written as follows:

$$\dot{\hat{z}} = A\hat{z} + Bu_d(t) + L(y - \hat{y})$$
$$\hat{y} = C\hat{z} \quad (15)$$

The matrix form of equation (15) is given by

$$\begin{pmatrix}\dot{\hat{z}}_1\\ \dot{\hat{z}}_2\end{pmatrix} = \begin{pmatrix}0 & 1\\ 0 & 0\end{pmatrix}\begin{pmatrix}\hat{z}_1\\ \hat{z}_2\end{pmatrix} + \begin{pmatrix}b\\ 0\end{pmatrix}u_d(t) + \begin{pmatrix}\beta_1\\ \beta_2\end{pmatrix}(y - \hat{y}) \quad (16)$$

Then, equation (16) becomes

$$\dot{\hat{z}}_1 = \hat{z}_2 + bu_d(t) - \beta_1(\hat{z}_1 - i_{ds})$$
$$\dot{\hat{z}}_2 = -\beta_2(\hat{z}_1 - i_{ds}) \quad (17)$$

where β_1 and β_2 are the gains of ESO, $\hat{z}_1$ is the estimate of real current i_{ds} and $\hat{z}_2$ is the estimate of generalized disturbance $f_{ds}(t)$.

The ESO gains $\beta_1 = 2\omega_0$ and $\beta_2 = \omega_0^2$ are determined based on bandwidth parameterization.

Therefore, estimated states are specified by

$$\dot{\hat{z}}_1 = \hat{z}_2 + \frac{1}{L}u_d(t) - 2\omega_0(\hat{z}_1 - i_{ds})$$
$$\dot{\hat{z}}_2 = -\omega_0^2(\hat{z}_1 - i_{ds}) \quad (18)$$

The estimated states $\hat{z}_1$ and $\hat{z}_2$ can track and , respectively, with fine tuning of observer bandwidth.

STEP 4: Development of control law for dq axes current to reject the disturbances.

The control law is designed as given below to terminate the lumped disturbance

$$v_{ds}^* = \frac{v_{ds}^0 - \hat{z}_2}{b_0}$$
$$v_{ds}^0 = k_p(i_{ds}^* - \hat{z}_1) \quad (19)$$

where i_{ds}^* is the reference direct axis component of stator current and v_{qs}^0 is the converter control signal.

Similarly, the control law for q-axis current is

$$v_{qs}^* = \frac{v_{qs}^0 - \hat{z}_2}{b}$$
$$v_{qs}^0 = k_p(i_{qs}^* - \hat{z}_1) \quad (20)$$

The current controller using ADRC for *d*-axis and *q*-axis is displayed in Figure. 6 and Figure 7

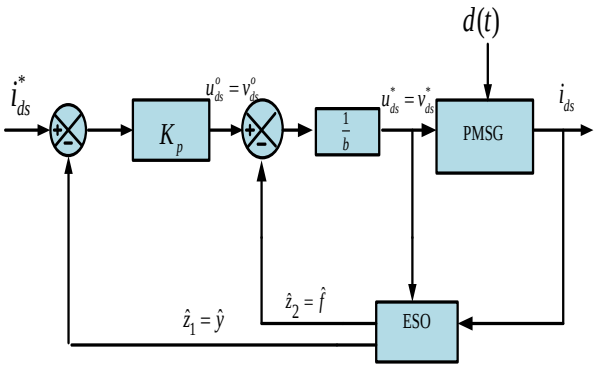

Figure 6. *d*-axis inner current controller using ADRC

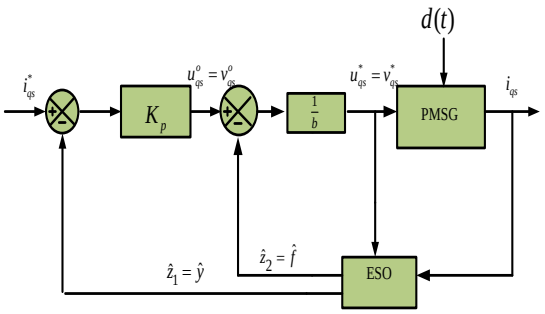

Figure 7. *q*-axis inner current controller using ADRC

3.5. Proposed ADRC Scheme for Utility Side Converter

The schematic block diagram of utility side inverter is exhibited in Fig. 8. The main aim of the GSC is to keep the DC link capacitor voltage at the reference and control the reactive power flow between GSC and main grid.

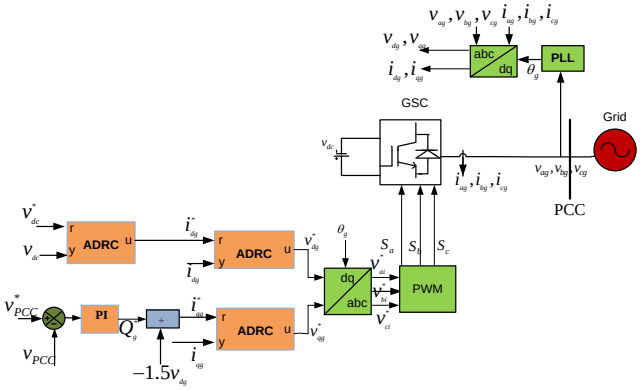

Figure 8. Block diagram of grid side converter using ADRC

In normal operating grid circumstances, the reference reactive power exchanged by the machine with power grid through the GSC is set to zero and the GSC operates at power factor of unity. The DC link loop produces the d-axis reference current, whereas the PCC voltage control loop creates the q-axis reference current. In contrast, the reference component of quadrature grid current is determined by reference reactive power. The actual and reference grid currents in dq frame are fed to the inner current loop. The dq reference voltage signals are converted by dq/abc transformation and changed to abc reference voltage signals. To produce the gate pulses for GSC, the reference voltage signals are directed to PWM. The control signals are modified to regulate the real and reactive current to track reference grid currents.

3.6. Mathematical Framework of ADRC Scheme for Utility Side Converter

The grid voltage in dq frame is specified by

$$v_{dg} = Ri_{dg} + L_g \frac{di_{dg}}{dt} - \omega_e L_g i_{qg} + v_{di}$$
$$v_{qg} = Ri_{qg} + L_g \frac{di_{qg}}{dt} + \omega_e L_g i_{dg} + v_{qi} \quad (21)$$

Equation (21) can be written as follows:

$$L_g \frac{di_{dg}}{dt} = v_{dg} - i_{dg}R_g + \omega_e L_g i_{qg} - v_{di}$$
$$L_g \frac{di_{qg}}{dt} = v_{qg} - i_{qg}R_g - \omega_e L_g i_{dg} - v_{qi} \quad (22)$$

Equation (22) indicates that grid voltage in *d*-axis is affected by grid current in *q*-axis, while grid voltage in *q*-axis is influenced by grid current in d-axis. This cross coupling effect on *dq*-axes results in difficulty to control i_{dg} and i_{qg}, respectively.Equation (22) is expressed by

$$\frac{di_{dg}}{dt} = -\frac{R_g}{L_g} i_{dg} + \frac{1}{L_g} v_{dg} + \omega_e i_{qg} - \frac{1}{L_g} v_{di}$$
$$\frac{di_{qg}}{dt} = -\frac{R_g}{L_g} i_{qg} + \frac{1}{L_g} v_{dg} - \omega_e i_{dg} - \frac{1}{L_g} v_{qi} \quad (23)$$

Equation (23) can be expressed by

$$\dot{i}_{dg} = f\left(i_{dg}, t\right) - \frac{1}{L_g} v_{di}$$
$$\dot{i}_{qg} = f\left(i_{qg}, t\right) - \frac{1}{L_g} v_{qi} \quad (24)$$

where $f\left(i_{dg}, t\right)$ and $f\left(i_{qg}, t\right)$ signify the internal system dynamics with grid parametric deviations and cross-coupled terms. Where

$$f\left(i_{dg}, t\right) = \left(-\frac{R_g}{L_g} i_{dg} + \frac{1}{L_g} v_{dg} + \omega_e i_{qg} \right)$$
$$f\left(i_{qg}, t\right) = \left(-\frac{R_g}{L_g} i_{qg} + \frac{1}{L_g} v_{qg} - \omega_e i_{dg} \right)$$

The system parameter (b) and control signal (u) in dq current loop for GSC is provided by

$$b = -\frac{1}{L_g}$$
$$v_{dg} = u_d$$
$$v_{qg} = u_q \quad (25)$$

The *dq*-axes grid current with external perturbation $d(t)$ is

$$\dot{i}_{dg} = f\left(i_{dg}, t\right) + d(t) + bu_d$$
$$\dot{i}_{qg} = f\left(i_{qg}, t\right) + d(t) + bu_q \quad (26)$$

The generalized disturbance for grid current in *dq*-axes involving the cumulative result of internal and external disturbances is provided by

$$f_{dg}(t) = f\left(i_{dg}, t\right) + d(t)$$
$$f_{qg}(t) = f\left(i_{qg}, t\right) + d(t) \quad (27)$$

Hence, equation (27) is given by

$$\dot{i}_{dg} = f_{dg}(t) + bu_d(t)$$
$$\dot{i}_{qg} = f_{qg}(t) + bu_q(t) \quad (28)$$

3.7. Mathematical Framework of ADRC in the dq-axes current loop

STEP 1: The canonical form of ADRC is given by
The grid current in *d*-axis from equation (28) is specified by

$$\dot{i}_{dg} = f_{dg}(t) + bu_d(t) \quad (29)$$

STEP 2: The formaulation of the state space model is given:
The state space model is supported by:

$$\dot{x} = Ax + Bu_d(t)$$
$$y = cx \quad (30)$$

where $A = \begin{pmatrix} 0 & 1 \\ 0 & 1 \end{pmatrix}; B = \begin{pmatrix} 1 \\ 0 \end{pmatrix}; C = (1)$

STEP 3: Development of ESO
The ESO is built to guess the states and lumped disturbance

$$\dot{\hat{z}} = A\hat{z} + Bu + L(y - \hat{y})$$
$$\hat{y} = C\hat{z} \quad (31)$$

The estimated states from the extended state observer from equation (31) is written as follows:

$$\begin{pmatrix} \dot{\hat{z}}_1 \\ \dot{\hat{z}}_2 \end{pmatrix} = \begin{pmatrix} 0 & 1 \\ 0 & 0 \end{pmatrix} \begin{pmatrix} \hat{z}_1 \\ \hat{z}_2 \end{pmatrix} + \begin{pmatrix} b \\ 0 \end{pmatrix} u_d(t) + \begin{pmatrix} \beta_1 \\ \beta_2 \end{pmatrix} \left(y - \hat{y}\right) \quad (32)$$

where $\hat{z}_1$ is the estimate state of *d*-axis current and $\hat{z}_2$ is the estimated state of lumped disturbance.
The new estimated states with observer gains $\beta_1 = 2\omega_o$; $\beta_2 = \omega_0^2$ are given below:

$$\dot{\hat{z}}_1 = \hat{z}_2 + \frac{1}{L} u_d(t) - 2\omega_0(\hat{z}_1 - i_{dg})$$
$$\dot{\hat{z}}_2 = -\omega_o{}^2(\hat{z}_1 - i_{dg}) \quad (33)$$

STEP 4: Development of the control law to compensate the disturbances. To reject the total disturbance, the control law is established as follows:

$$u_d^* = \frac{u_{d0} - \hat{z}_2}{b}$$
$$u_d^0 = k_p(i_{dg}^* - \hat{z}_1) \quad (34)$$

where

$$u_d = v_{dg}$$

Thus, for d-axis current controller, the control law is written by:

$$v_{dg} = \frac{v_{dg}^o - \hat{z}_2}{b_0}$$
$$v_{dg}^* = k_p(i_{dg}^* - \hat{z}_1) \quad (35)$$

where k_p is the gain of the controller and i_{dg}^* is the reference *d*-axis current, and v_{dg} is inverter control input in *d*-axis

current controller. Similarly, for the *q*-axis current controller, we have:

$$v_{qg} = \frac{v_{q0} - \hat{z}_2}{b}$$
$$v_{qg}^0 = k_p(i_{qg}^* - i_{qg}) \quad (36)$$

where i_q^* indicates the reference *q*-axis current and v_{qg} is the inverter control input for *q*-axis current controller. The structure of ADRC for the *dq*-axes current loop is shown in Fig. 9 and Fig. 10, and the DC link voltage controller using ADRC is shown in Fig. 11.

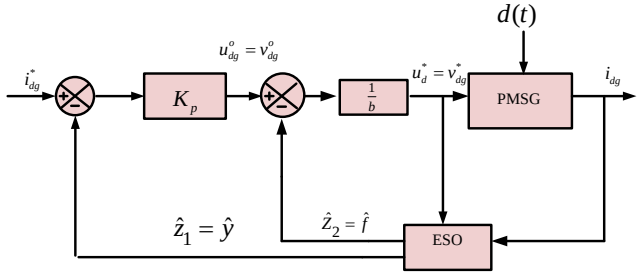

Figure 9. d-axis inner current controller for GSC using ADRC

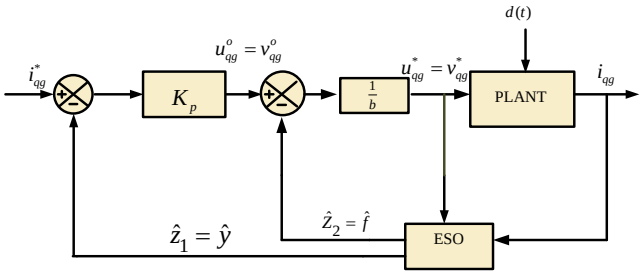

Figure 10. q-axis inner current controller for GSC using ADRC

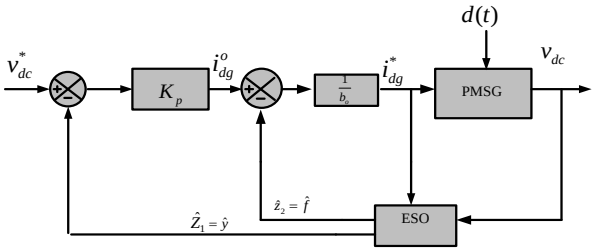

Figure 11. DC-Link voltage controller using ADRC

3.8. Tuning of Controller Parameters

The present work employs the Empirical tuning method to adjust the parameters. Empirical tuning proves to be a practical and effective approach for optimizing ADRC controllers in real-world scenarios. This method utilizes data from simulation results and practical insights to customize the controller's parameters, thereby ensuring robust performance in the presence of uncertainties and disturbances.

3.8.1. Tuning of observer bandwidth

Observer bandwidth is determined by observer gains. The poles of the Extended State Observer (ESO) are configured, and the characteristic equation of the ESO can be obtained. In this method, observer gains are selected so that the roots of the characteristic polynomial of the observer lie on the left half of the s-plane and are located at $\beta_1=2\omega_0$ and $\beta_2= \omega_0^2$. The stability condition requires that the roots of the characteristic equation are in the left half of the s-plane. Ensuring $\beta_1 > 0$ and $\beta_2 > 0$ guarantees controller stability. To enhance the stability margin of the system, the roots of the characteristic equation are kept away from the imaginary axis. With the appropriate selection of β_1 and β_2, the observer states Z_1 and Z_2 will track *y* and *f*, respectively. Increasing the observer bandwidth reduces the estimation errors of the ESO, but increases the noise sensitivity. An appropriate observer bandwidth should be tuned in a trade-off between the tracking performance and the noise tolerance.

3.8.2. Tuning of controller bandwidth

The controller gain, *kp*, is selected in such a way that the poles of the approximate closed-loop characteristic polynomial are positioned at $-\omega_c$, in accordance with the desired settling time. Moreover, with an increase in the controller bandwidth, the speed of the transient response rises, but the stability margin diminishes. Therefore, the controller bandwidth is determined to strike a balance between the transient response and robustness. Generally, we opt for ω_0 to be 3 to 7 times ω_c. Hence, ω_c is the only one tuning parameter. ω_c =4/Tsettle where T_{settle} is the desired closed loop settling time.

4. RESULTS AND DISCUSSION

The test system, as depicted in Figure 12, is employed to assess the performance of the PMSG wind turbine. The PMSG is linked to the grid network through an extensive transmission line. The wind velocity is assumed to be constant throughout the simulation. Various case studies are conducted to examine the efficiency of the proposed scheme under external grid disturbances, including symmetrical fault, asymmetrical fault, voltage swell, wind speed variance, and internal disturbances. The parameters for the wind turbine and controller can be found in the Appendix.

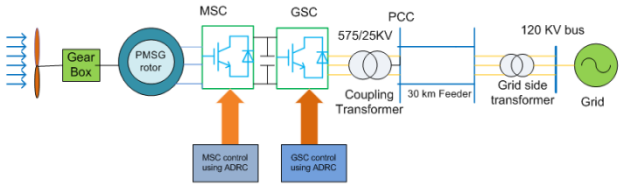

Figure 12. Test system under consideration

4.1. LVRT Enhancement of the grid tied wind turbine in symmetrical fault conditions using ADRC

The symmetrical fault is initiated at t=1s and is eliminated after 200 ms, as exposed in Fig. 13. The parameters of the system, including voltage at PCC, reactive power, active power, generator speed, torque, and DC link voltage, are displayed in Figure 13. The voltage response at PCC is revealed in Fig. 13(a). The proposed method's aim is to control the PCC voltage by adjusting the reactive power supplied into the grid. The PCC voltage drops due to a symmetrical fault at t=1 s, which results in a large voltage drop in the line between the grid and PCC. If the voltage drop is sustained for a considerable duration, then the wind turbine will be detached. After the fault is vanished, the voltage at PCC returns to its pre-fault state, as portrayed in Fig. 13(a). The proposed method improves the voltage at PCC to the normal state faster than PR and PI control schemes. The voltage at PCC is regulated by controlling reactive power injection by the grid-side inverter. The utility-side inverter of PMSG acts as a source of reactive power injection at PCC. The reactive power injection is zero in normal operating conditions, while the reactive power injection varies during fault conditions. As shown in Fig. 13(b), the reactive power distributed with the proposed scheme is higher than that of other control schemes, aiding in the restoration of PCC voltage to its pre-fault state. Another crucial grid code requirement is the prompt restoration of active power to its

normal state after the fault dissipates. As illustrated in Fig. 13(c), real power experiences a slight decline during a fault condition and swiftly returns to the pre-fault state once the fault disappears. The proposed scheme successfully restores it to a normal state more rapidly than both the resonant controller and a typical vector PI control scheme, as depicted in the figure. Fig. 13(d) illustrates rotor speed oscillations during a symmetrical fault disturbance. The mechanical torque surpasses the machine's torque at the fault's onset, causing an increase in the PMSG rotor speed. A sudden jump in the wind generator's rotational speed occurs due to the disparity between the wind turbine's electrical and mechanical power, leading to vibrations in the wind turbine's mechanical system. As depicted in Fig. 13(d), the proposed technique exhibits a smaller speed deviation and proves to be more effective in damping rotor speed oscillations compared to PR and PI control strategies. Fig. 13(e) illustrates the electromagnetic torque response in the presence of a symmetrical fault condition. Mechanical shaft vibration induces significant mechanical stress and has the potential to disconnect the wind turbine from the grid. In the event of a grid interruption, the proposed approach excels in mitigating mechanical vibrations on the turbine shaft, thereby extending its operational lifespan. Consequently, the suggested approach contributes to maintaining torque control more stably compared to the PR and vector PI control schemes. During a fault condition, the generator continues to generate electrical power, while delivered grid power decreases. Due to this condition, unbalanced power is stored in the dc-link interface. This unbalanced power causes a rise in the dc-link voltage at the dc-link interface. The converter switches, and the dc-link capacitor get destroyed due to excess voltage at the dc link. Subsequently, a wind turbine gets disconnected from the external grid system, leading to voltage stability issues. From Fig.13(f), it is observed that a large overshoot is seen in dc-link voltage with the vector PI controller. However, the proposed scheme offers less deviation in dc-link voltage from the reference voltage and stays within the safety limits, closely tracking its reference. The PMSG stator current variation using ADRC, PR, and PI control methods is depicted in Fig.13(g), Fig.13(h), and Fig.13(i). During t=1 s to t=1.2 s, the stator current is controlled within the nominal value, thus preventing high stator current into the converter, thereby avoiding damage to converters.

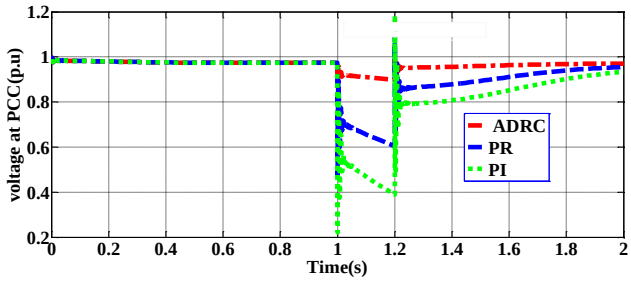

(a)

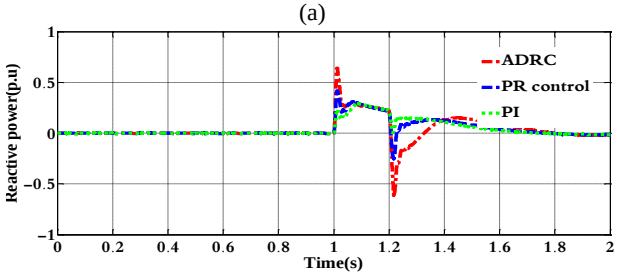

(b)

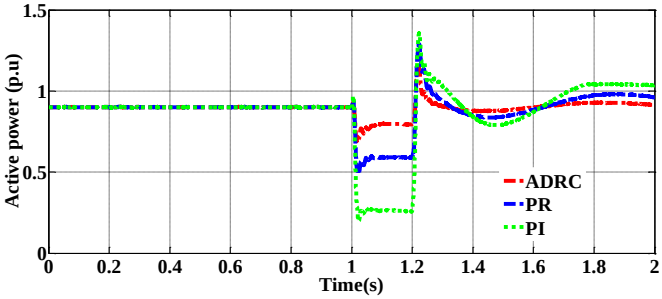

(c)

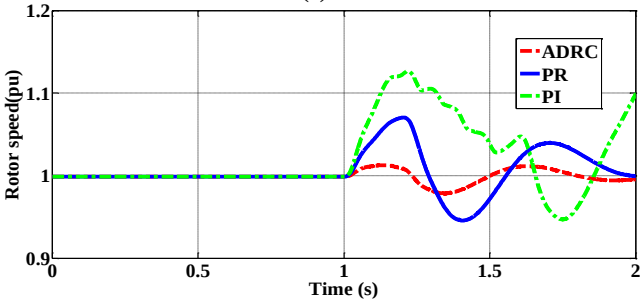

(d)

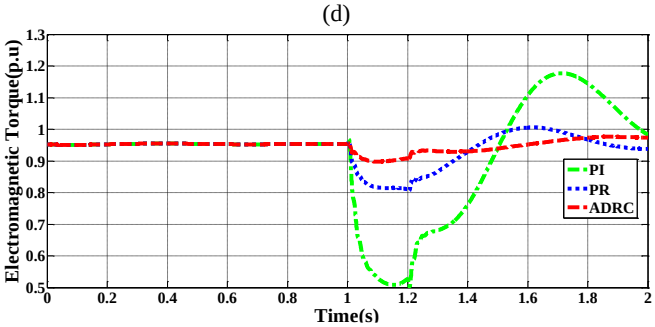

(e)

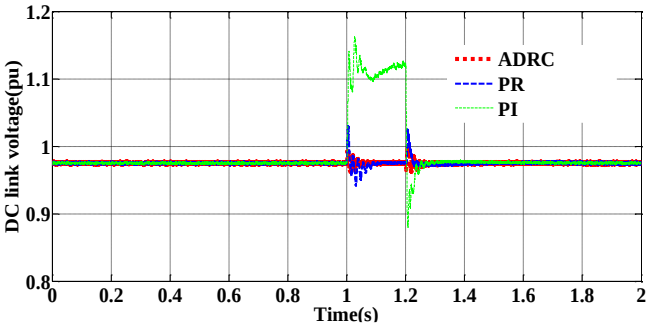

(f)

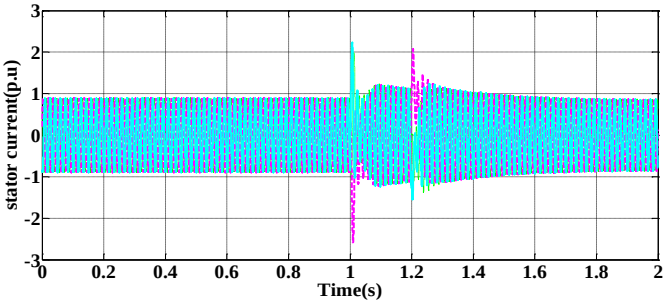

(g)

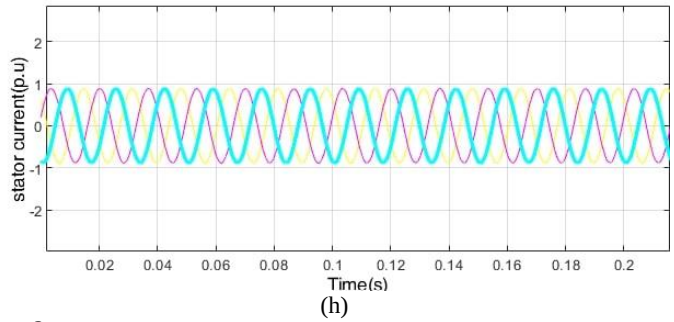

(h)

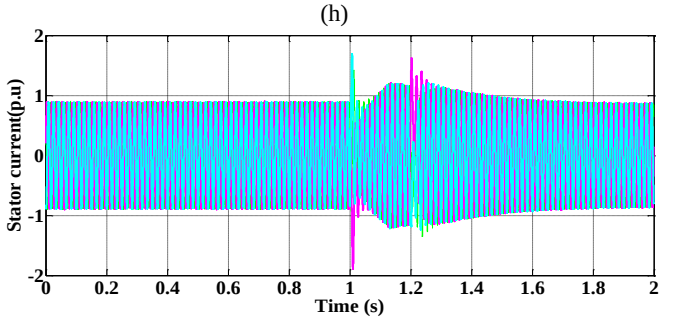

(i)

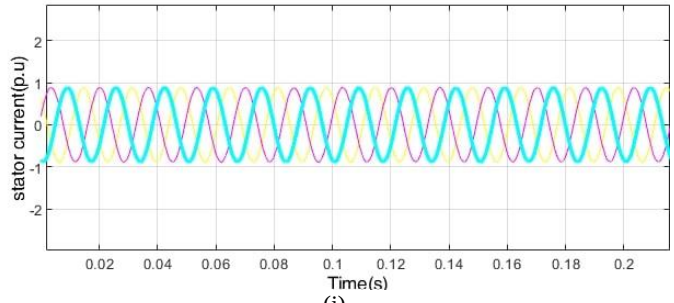

(j)

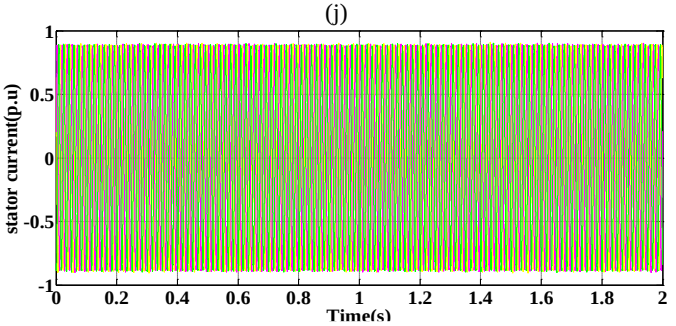

(k)

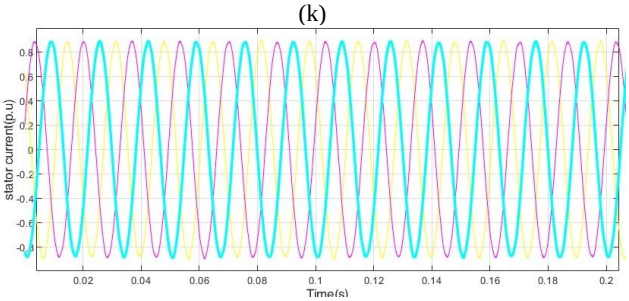

(l)

Figure 13. Simulation results for the grid tied wind turbine in symmetrical fault conditions using ADRC (a) Voltage at PCC, (b) Reactive power, (c) Real power, (d) Rotor speed, (e) Torque, (f) DC link voltage, (g) Stator current using PI, (h) Zoomed version of Stator current using PI, (i) Stator current using PR, (j) Stator current using PR, (k) Stator current using ADRC, (l) Stator current using ADRC.

4.2. LVRT improvement of grid connected wind energy in LG fault condition using ADRC

At t=1 s, an unsymmetrical fault occurs for a duration of 200 ms. As shown in Fig. 14(a), the PCC voltage decreases during the unsymmetrical fault. The voltage at PCC rapidly returns to its pre-fault level after fault clearance. It is evident from Fig. 14(a) that the voltage at PCC increases much more with the proposed control strategy compared to PI and PR control strategies.

Fig. 14(b) displays the reactive power supplied by the GSC. The reactive power provided by the GSC, utilizing the proposed control scheme, exceeds that of PR and PI controllers. This enhancement contributes to the recovery of PCC voltage to its pre-fault state under fault conditions. Fig. 14(c) displays the active power profile in the presence of asymmetric fault conditions.

From Fig. 14(c), it is detected that the real power delivered to the grid slightly decreases, indicating that the suggested system has the lowest power relative to the PR and vector PI control methods. Fig. 14(d) illustrates the response of rotor speed under LG fault conditions. As shown in Fig. 14(d), there is a noticeable increase in rotor speed oscillations during an LG fault.

The rotor speed fluctuates more, and stabilization is not achieved quickly under a conventional controller. In contrast, the proposed method minimizes rotor speed oscillations more effectively than the resonant controller and PI controller.

Fig. 14(e) indicates the waveform of electromagnetic torque under a line-to-ground fault. As shown in Fig. 14(e), it is observed that with the proposed controller in operation, electromagnetic torque fluctuation is relatively low, thereby minimizing stress on the generator turbine mechanical unit.

In Fig. 14(f), the DC link voltage experiences significant oscillation in the transient state and returns to the pre-fault state after the fault disappears. It can be seen from Fig. 14(f) that the proposed approach minimizes DC link voltage variation faster than PI and PR control methods. Fig. 14(g), Fig. 14(h), and Fig. 14(i) show the PMSG stator current variation using ADRC, PR, and PI control approaches, respectively, under asymmetrical fault conditions.

During the time interval t=1 s to t=1.2 s, the stator current is maintained within the nominal range, preventing high stator current from entering the converter and protecting it from damage.

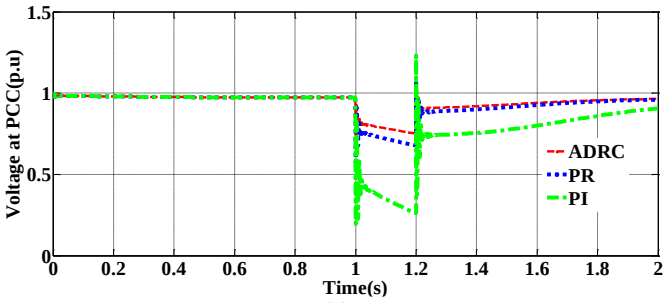

(a)

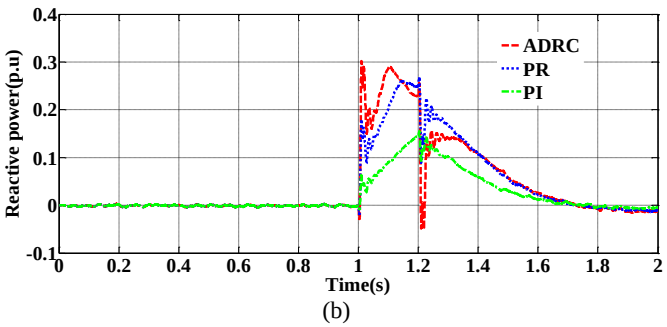

(b)

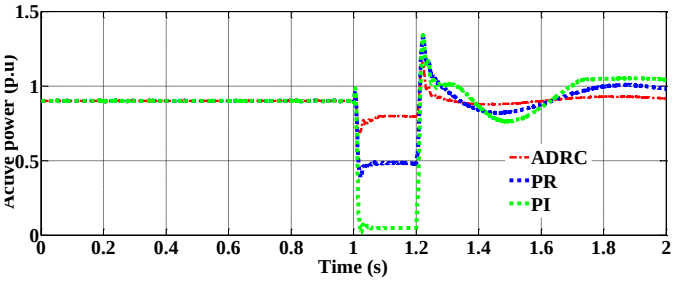

(c)

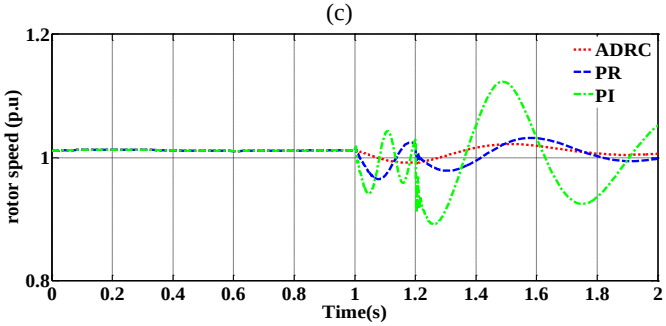

(d)

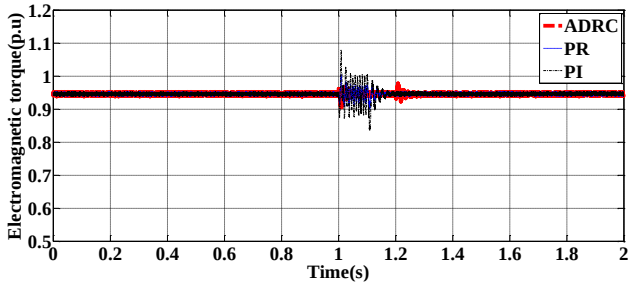

(e)

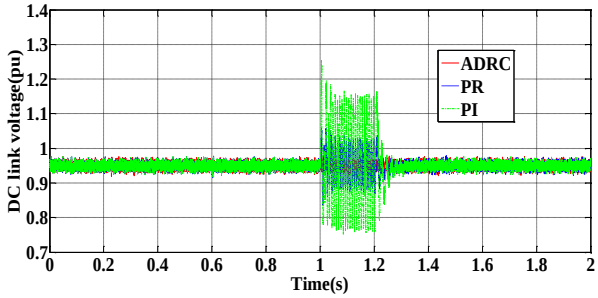

(f)

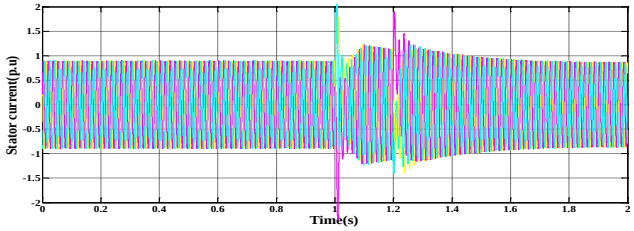

(g)

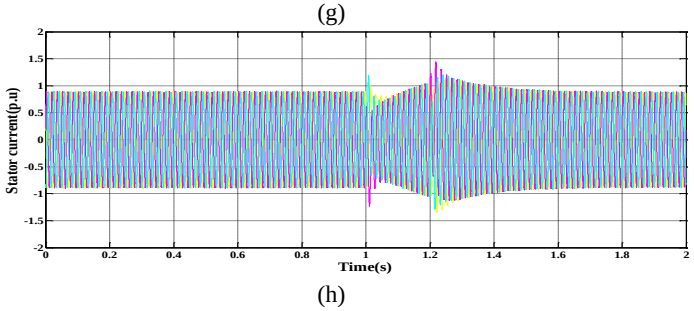

(h)

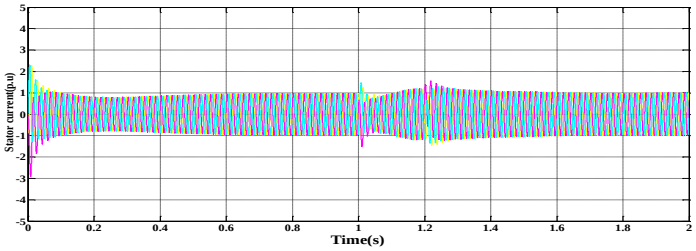

(i)

Figure 14. Simulation waveforms for the grid tied wind turbine in asymmetrical fault conditions using ADRC (a) Voltage waveform at PCC, (b) Reactive power waveform, (c) Real power response, (d) Rotor speed, (e) Torque waveform, (f) DC link voltage, (g) Stator current using PI, (h) Stator current using PR, (i) Stator current using ADRC.

4.3. HVRT capability of grid connected wind energy in voltage swell scenario using ADRC

In this case, a voltage swell occurs on the grid side. Modern grid codes stipulate that wind turbines must endure a voltage rise for a defined period, known as High Voltage Ride-Through (HVRT) capability. The proposed grid-side controller is designed to meet HVRT requirements by absorbing reactive power. The voltage profile at the Point of Common Coupling (PCC) is depicted in Fig. 15(a). Observing Fig. 15(a), it is evident that the proposed controller effectively reduces voltage rise during a swell. Additionally, the voltage recovers rapidly with the proposed control after the fault has dissipated, in comparison to conventional vector PI and PR controllers. Consequently, the proposed method prevents the disconnection of the wind turbine from the grid.

The reactive power observed at the Point of Common Coupling (PCC) is presented in Fig. 15(b). The reactive power observed by the utility-side inverter is high with the proposed scheme, preventing an increase in voltage during grid disturbance conditions, while the reactive power absorption is low with the PI and PR control scheme. From the results, it is noticed that the wind turbine can withstand over-voltage conditions by successfully absorbing reactive current, thereby enhancing the High Voltage Ride Through (HVRT) requirement.

Fig. 15(c) displays the real power waveform under the state of a voltage rise condition. Before the grid interruption happens, the real output power is retained around 1 p.u. The active power pumped into the grid grows during the voltage swell and is controlled at the reference value using the proposed control after the fault is removed.

Fig. 15(d) depicts the waveform of rotor speed under a voltage rise condition. The results prove that the proposed scheme has demonstrated improved performance in reducing overshoot and steady-state error in rotor speed compared to PR and conventional PI controllers. The reduced steady-state error provides good mechanical stability to the wind energy system under abnormal grid conditions.

The Permanent Magnet Synchronous Generator (PMSG) electromagnetic torque response is shown in Fig. 15(e) when the grid is subjected to a voltage swell disturbance. Fig. 15(e) shows that the proposed scheme ensures the least variations in torque oscillations compared to PR and PI control. The response of the DC link voltage waveform is presented in Fig. 15(f). With the proposed system, the overshoot present in DC-link voltage is significantly reduced. As seen in Fig. 15(f), the proposed solution aims to keep the DC link voltage relatively steady compared to PR and PI control methods.

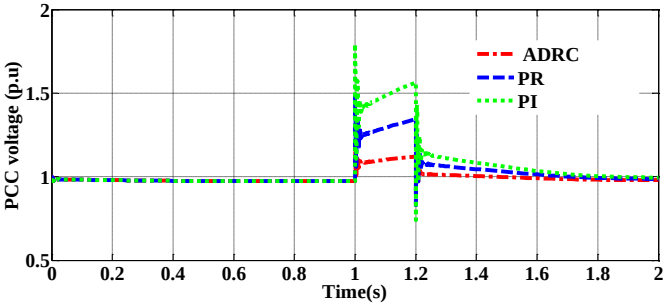

(a)

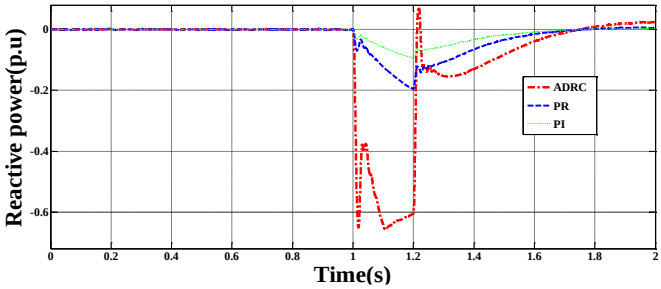

(b)

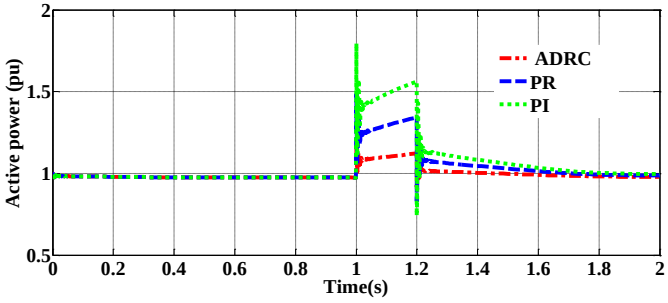

(c)

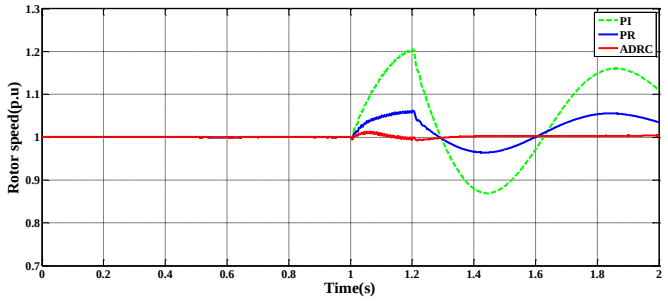

(d)

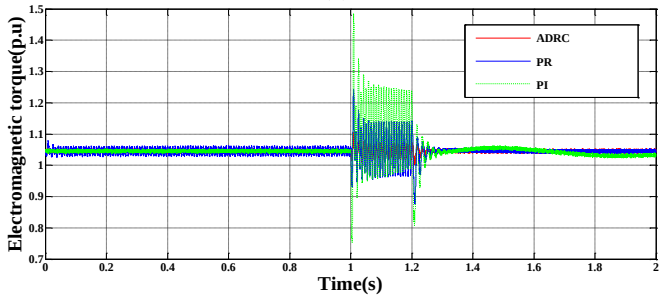

(e)

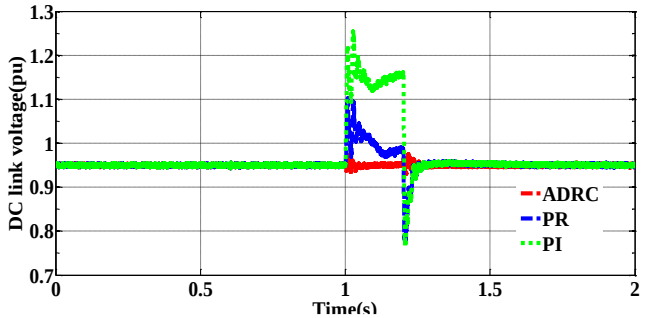

(f)

Figure 15. Simulation results for grid tied PMSG wind turbine under voltage rise scenario using ADRC (a) Voltage response at PCC, (b) Reactive power response, (c) Real power waveform, (d) rotor speed waveform, (e) Electromagnetic torque, and (f) dc link voltage waveform.

4.4. Peformance Assessment of the Proposed Control Scheme

The comparison of system parameters in terms of rise time, settling time, overshoot, and steady-state error has been tabulated below. All system parameters are in per unit values. Table 1 presents the performance assessment of the proposed controller under adverse grid conditions. From Table 1, it is noticed that there has been a substantial decrease in steady-state error, overshoot, rise time, and settling time for machine and grid parameters using ADRC compared to PR and PI controllers.

4.5. Peformance improvement of the grid tied PMSG Wind turbine in distorted Grid and parameter uncertainities

In this scenario, we evaluate the robust performance of the proposed control scheme by considering the distorted harmonic grid as well as parametric uncertainties. The grid voltage response in distorted grid conditions is depicted in figure 16(a). Harmonically distorted voltage induces pulsations in stator and grid current, leading to fluctuations in PMSG active and reactive power and DC link voltage. The pulsations in PMSG active power are illustrated in figure 16(b). Notably, the proposed ADRC minimizes the pulsations in real power delivered to the grid, closely adhering to the rated active power, as shown in Fig. 16(b). Fig. 16(c) showcases the reactive power provided to the grid from the utility-side converter under distorted grid and machine parametric variations. The reactive power supplied to the grid is closely maintained at the reference reactive power, ensuring control at unity power factor using ADRC, as revealed in Fig. 16(c). Both Fig. 16(b) and Fig. 16(c) confirm that real and reactive power introduced into the grid have been maintained at their reference values. Fig. 16(d) presents the waveform of DC link voltage with the proposed and PR, PI control schemes. The fluctuations in DC link voltage are minimized using ADRC, providing satisfactory tracking performance in controlling DC link voltage at its reference without significant overshoot when compared to PR and PI controllers. The grid current is displayed in Fig. 16(e)-Fig. 16(g) using ADRC, PR, and PI controllers. The results indicate that the grid current using the proposed method is well-balanced in distorted grid conditions compared to PR and PI controllers.

Table 1. Performance Assessment of controller under Adverse Grid conditions

Controller	Overshoot(%)				Rise time(s)				Settling Time(s)				Steady state error(%)			
	V	P	T	V_{dc}	V	P	T	V_{dc}	V	P	T	V_{dc}	V	P	T	Vdc
CASE 1: Symmetrical fault condition																
PI	0.6	0.6	0.5	0.1	2	1.8	1.1	1.1	1.82	1.9	2	1.23	0.3	0.2	0.03	0.02
PR	0.4	0.5	0.2	0.2	1.8	1.6	1.1	1	1.61	1.8	1.9	1.22	0.2	0.1	0.02	0.01
ADRC	0.1	0.1	0.05	0.01	1.6	1.4	1.1	1	1.45	1.4	1.4	1.22	0.1	0.1	0.02	0.01
CASE 2: Asymmetrical fault condition																
PI	0.7	1.4	0.1	0.2	1.2	1.2	1.1	1.1	1.9	1.6	1.62	1.22	0.2	0.05	0.01	0.01
PR	0.2	1.3	0.02	0.1	1.2	1.2	1.1	1.1	1.65	1.4	1.61	1.21	0.15	0.04	0	0
ADRC	0.1	1.2	0.01	0.01	1.2	1.2	1.1	1.1	1.6	1.3	1.61	1.21	0.1	0.04	0	0
CASE 3: Voltage swell condition																
PI	0.5	1.8	1.4	0.12	1.1	1.1	1.6	1.1	1.6	1.6	1.6	1.21	0.1	0.01	0.01	0.01
PR	0.3	1.5	1.2	0.1	1.1	1.1	1.6	1.1	1.4	1.4	1.6	1.21	0	0.01	0	0
ADRC	0.2	1.2	1.1	0.1	1.1	1.1	1.6	1.1	1.21	1.2	1.6	1.23	0	0	0	0

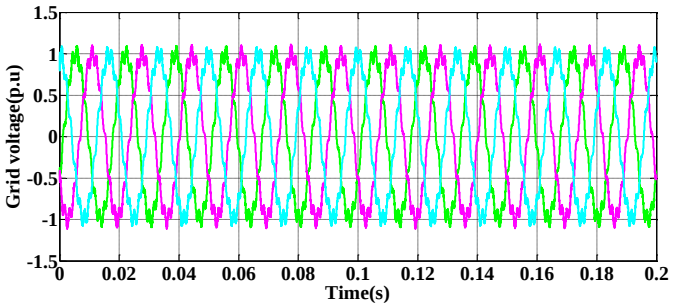

(a)

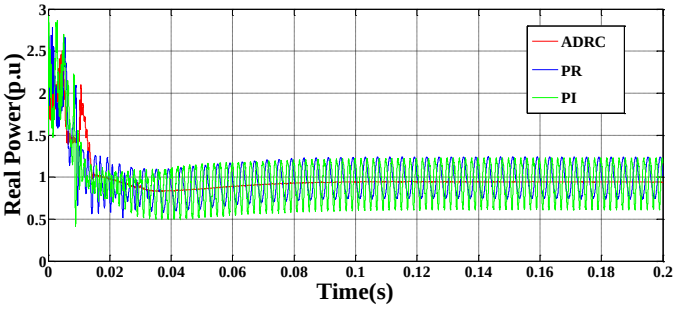

(b)

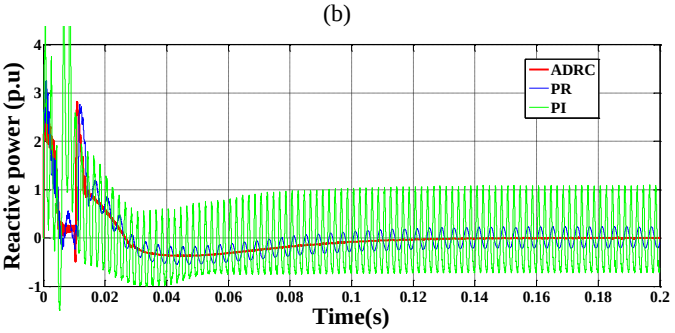

(c)

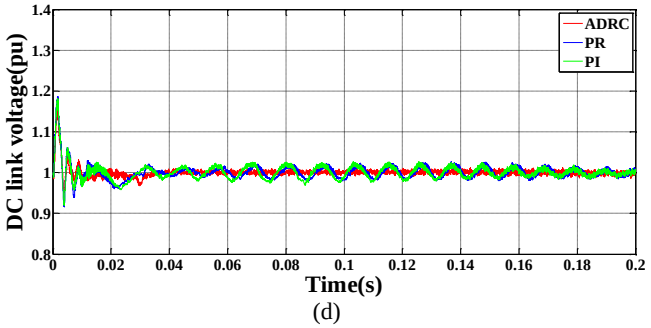

(d)

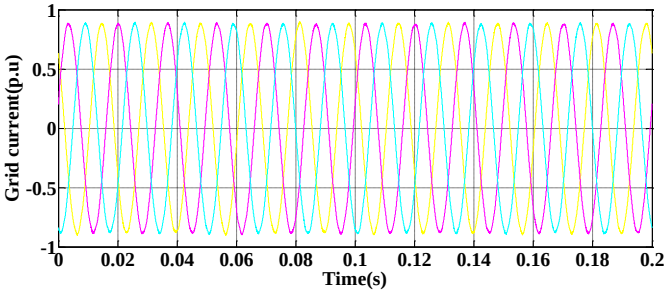

(e)

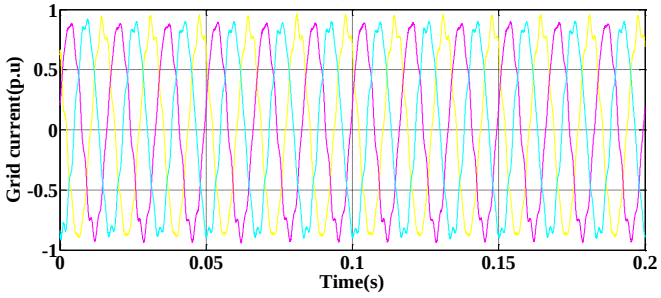

(f)

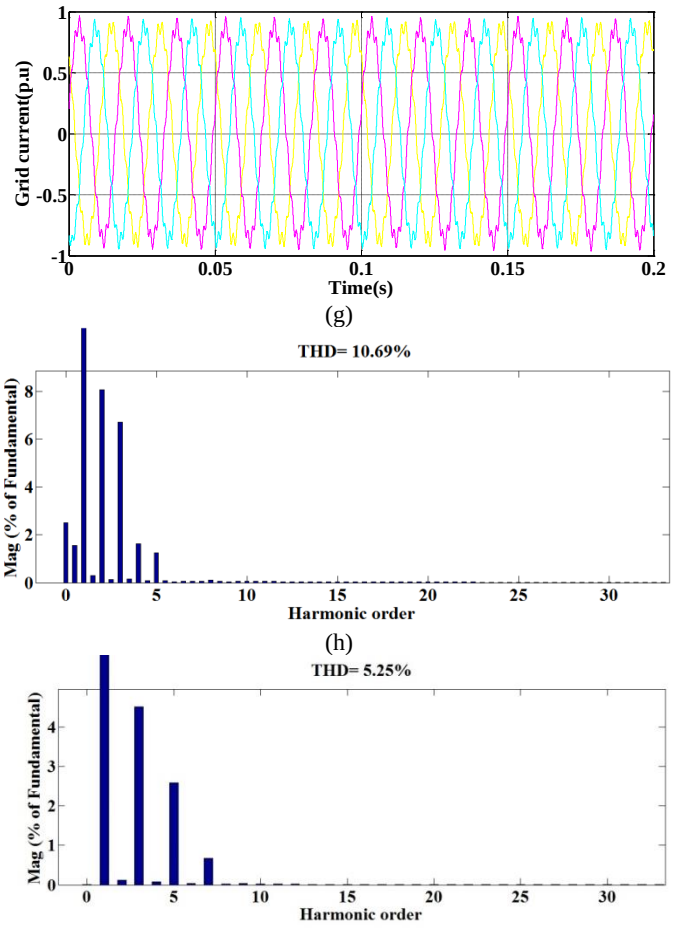

Figure 16. Simulation results in distorted grid and parametric uncertainties: (a) distorted grid voltage, (b) active power, (c) reactive Power, (d) DC link voltage, (e) distorted grid current using ADRC, (f) distorted grid current using PR, (g) distorted grid current using PI, (h) THD of grid voltage, (i) THD of grid current using PR.

4.6. Peformance improvement of the grid tied PMSG Wind turbine with Wind Speed Variations

The step rise and drop in wind speed variation are considered at t=1 s and t=2 s, as presented in Fig. 17(a). Fig. 17(b) demonstrates the effectiveness of the suggested approach in ensuring optimum power coefficients for reaching optimal electricity production. The power coefficient Cpmax tracks the optimum value with only a few minor variations for the suggested ADRC, while it deviates slightly from its reference using PR and PI, respectively.

Fig. 17(c) displays the DC-link voltage response to a step change in wind velocity variation. The proposed approach exhibits an improved response and low overshoot compared to PR and PI control schemes. The reactive power provided to the grid is shown in Fig. 17(d) under variable wind speed conditions. At t=1 s, the PI Controller yields higher reactive power variation with a larger settling time, whereas the ADRC-based method exhibits less overshoot in reactive power with a faster settling time. Fig.17(e) represents the optimal tip speed ratio under varying wind velocity conditions. The tip speed ratio slightly increases with minimal fluctuation in wind speed variation. In contrast, with the proposed ADRC and PR controllers, the tip speed ratio closely tracks the reference well under wind speed turbulence. Fig. 17(f) demonstrates that with the recommended ADRC, the rotor velocity tracks its optimal value, whereas at t=1 s, it starts to deviate from its optimal value with PR and PI control. Compared to other methods, the proposed method shows a fast response with minimal steady-state oscillations.

The dq-axes stator and grid currents are represented in Fig. 17(g) and Fig. 17(h). These components are appropriately controlled around their reference values in varying wind conditions using the proposed ADRC.

In this scenario, we evaluate the robust performance of the proposed control scheme by considering the distorted harmonic grid as well as parametric uncertainties. The grid voltage response in distorted grid conditions is depicted in figure 16(a). Harmonically distorted voltage induces pulsations in stator and grid current.

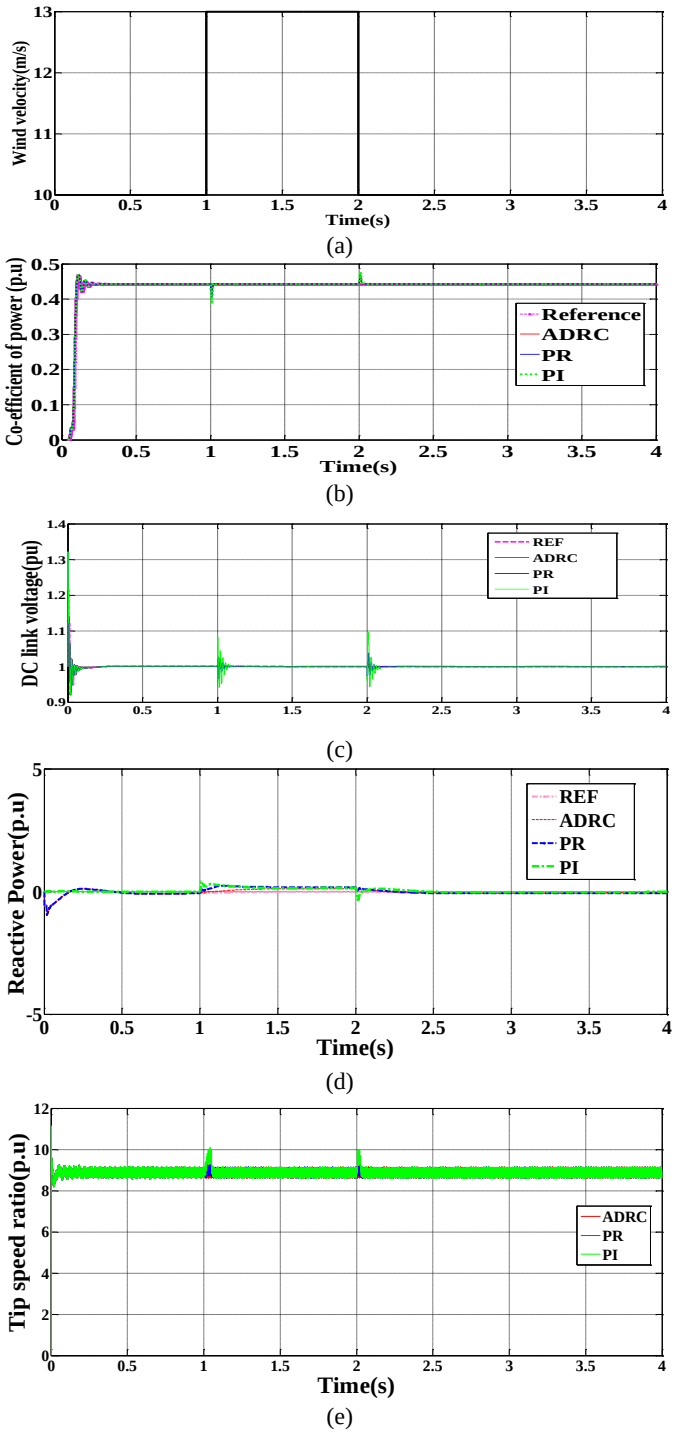

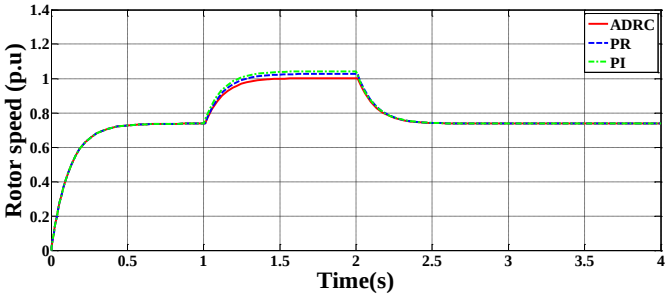

(f)

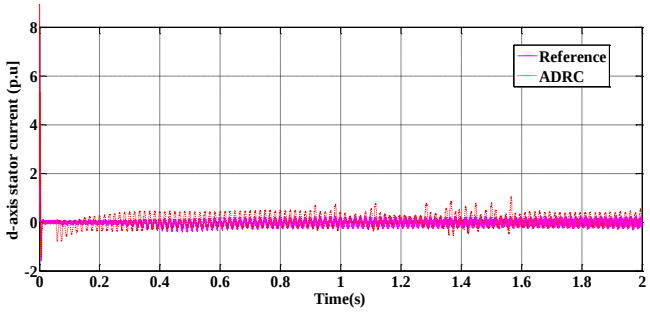

(g)

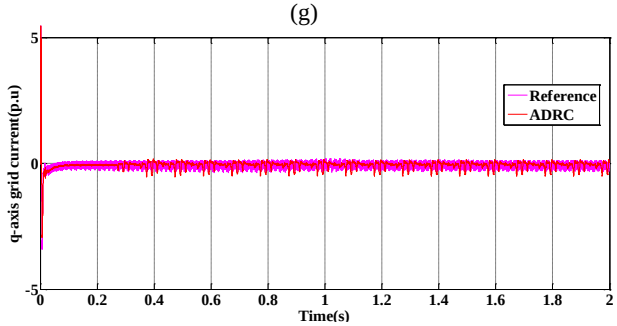

(h)

Figure 17. Simulation waveforms under step wind speed conditions (a) variation of wind speed (b) Coefficient of power (c) DC link voltage (d) reactive power delivered (e) tip speed ratio (f) Rotor speed (g) d-axis stator current (h) q-axis grid current.

5. CONCLUSIONS

The effectiveness of the proposed controller was tested to improve low voltage and high voltage ride-through capability of the grid tied wind turbine under various grid disturbance conditions. The mentioned effectiveness was also tested in symmetrical and asymmetrical fault conditions.

Findings

- The drop in PCC voltage due to a fault condition is maintained at the desired level by controlling the reactive power exchange between the grid-side converter and the grid. The proposed controller limits the rise in DC link, rotor speed, electromagnetic torque, and stator current in various fault conditions, thereby enabling the wind turbine to remain connected under abnormal grid conditions to meet the Low Voltage Grid Code requirements.
- The rise in PCC voltage due to a voltage swell scenario is maintained at the desired level by controlling the reactive power. The proposed controller also limits the rise in DC link, rotor speed, electromagnetic torque, and stator current in voltage swell conditions, thereby enabling the wind turbine to remain connected to meet the High Voltage Grid Code requirements.
- From the results, it is perceived that there is a reduction in steady-state errors and reduced overshoot of machine and grid-side parameters. The simulation results illustrate that the proposed scheme can efficiently protect the system against high DC link voltage, stator current, speed, torque, and PCC voltage under grid fault conditions.
- The performance of grid-interfaced PMSG wind energy has been tested to enhance power quality under distorted grid conditions. The results reveal that the desired output grid current is effectively regulated and balanced. The harmonic distortion of the grid current waveform is well within acceptable limits.
- Finally, the Low Voltage Ride Through (LVRT) and High Voltage Ride Through (HVRT) capability has been assessed using performance measures such as Integral of Time multiplied by Absolute Error (ITAE) deviations. The proposed control technique yields the least index values; hence, the improvement is significant. The effectiveness of the proposed Active Disturbance Rejection Control (ADRC) structure has been compared with the vector PI and PR controller methods by considering the ITAE index.
- The test system, as depicted in Figure 12, is employed to assess the performance of the PMSG wind turbine. The PMSG is linked to the grid network through an extensive transmission.

Potential limitations

- Wind energy systems operate in dynamic environments with varying wind speeds and grid conditions. Incorrect tuning can lead to suboptimal performance and may not fully exploit the benefits of enhanced LVRT and HVRT capabilities.

Future work

- The investigation of the proposed controller for real-time grid interfaced PMSG wind energy can be validated in grid disturbances, variable wind, and load conditions by considering real time data, and the results obtained through simulation and real-time can be compared.

  By incorporating machine learning and deep learning approaches into the design and operation of grid-connected PMSG wind energy systems, it is possible to enhance their efficiency and reliability under varying wind and grid conditions, providing more flexible and responsive control of PMSG wind turbines. The proposed solutions can be validated through extensive field testing on actual wind energy installations. Field data can provide valuable insights into the real-world performance of the systems and help refine theoretical models and simulations

ACKNOWLEDGEMENT

The authors sincerely thank Shri Vishnu Engineering College for Women Bhimavaram (Autonomous) for providing required research facilities for carrying and completing the research work fruitfully.

NOMENCLATURE

k_p	Proportional gain
k_{ri}	Resonant gain
ω_r	Resonant frequency

i_{ds}, i_{qs}	*d*-axis and *q*-axis component of stator current
i_{dg}, i_{qg}	*d*-axis and *q*-axis component of grid current
v_{ds}, v_{qs}	*d*-axis and *q*-axis component of stator voltage
v_{ds}, v_{qs}	*d*-axis and *q*-axis component of stator voltage
ω_e	Electrical angular speed of the rotor
v_{dc}	dc link voltage
λ	Tip speed ratio
c_p	Coefficient of Power

REFERENCES

1. Abbey, C., & Joos, G. (2007). Supercapacitor Energy Storage for Wind Energy Applications. *IEEE Transactions on Industry Applications, 43(3),* 769-776. https://doi.org/10.1109/TIA.2007.897808
2. Alam, S., & Abido, M. (2018). Fault Ride Through Capability Enhancement of a Large-Scale PMSG Wind System with Bridge Type Fault Current Limiters. *Advances in Electrical and Computer Engineering, 18,* 43-50. https://doi.org/10.4316/AECE.2018.04006
3. Alepuz, S., Calle, A., Busquets-Monge, S., Kouro, S., & Wu, B. (2013). Use of Stored Energy in PMSG Rotor Inertia for Low-Voltage Ride-Through in Back-to-Back NPC Converter-Based Wind Power Systems. *IEEE Transactions on Industry Applications, 60(5),* 1787-1796. https://doi.org/10.1109/TIA.2013.2259291
4. Ayadi, M., & Derbel, N. (2017). Nonlinear adaptive backstepping control for variable speed wind energy conversion system-based permanent magnet synchronous generator. *International Journal of Advanced Manufacturing Technology, 92,* 39–46. https://doi.org/10.1007/s00170-017-0020-y
5. Belachew Desalegn, Desta Gebeyehu, Bimrew Tamrat (2023). Smoothing electric power production with DFIG-based wind energy conversion technology by employing a hybrid controller model. *Journal of Renewable Energy, 10,* 38-60, https://doi.org/10.1016/j.egyr.2023.06.004
6. Bolund, B., Bernhoff, H., & Leijon, M. (2007). Flywheel energy and power storage systems. *Renewable and Sustainable Energy Reviews, 11(2),* 235–258. https://doi.org/10.1016/j.rser.2005.04.003
7. Causebrook, A., Atkinson, D. J., & Jack, A. G. (2007). Fault Ride-Through of Large Wind Farms Using Series Dynamic Braking Resistors. *IEEE Transactions on Power Systems, 22(3),* 966-975. https://doi.org/10.1109/TPWRS.2007.901250
8. Cheikh, R., Menacer, A., Chrifi-Alaoui, L., & Bensmail, C. (2020). Robust nonlinear control via feedback linearization and Lyapunov theory for permanent magnet synchronous generator-based wind energy conversion system. *Frontiers in Energy, 14,* 180–191. https://doi.org/10.1007/s11708-019-0679-6
9. Chen, X., Yan, L., Zhou, X., & Sun, H. (2018). A Novel DVR-ESS-Embedded Wind-Energy Conversion System. *IEEE Transactions on Sustainable Energy, 9(3),* 1265-1274. https://doi.org/10.1109/TSTE.2017.2753962
10. Díaz-González, F., Sumper, A., Gomis-Bellmunt, O., & Bianchi, F. D. (2013). Energy management of flywheel-based energy storage device for wind power smoothing. *Applied Energy, 110,* 207–219. https://doi.org/10.1016/j.apenergy.2013.04.066
11. Ehsan Hosseini et al (2023) Control of Pitch Angle in Wind Turbine Based on Doubly Fed Induction Generator Using Fuzzy Logic Method. *Journal of Renewable Energy and Environment, 9(2),* 1-7.https://doi.org/10.30501/jree.2021.293546.1226
12. Elmouhi, Noureddine & Essadki, Ahmed & Elaimani, Hind. (2023). Fault tolerant control for DFIG wind turbine controlled by ADRC and optimized by genetic algorithm. *International Journal of Power Electronics and Drive Systems (IJPEDS). 14(3).*1382-1393. https://doi.org/10.11591/ijpeds.v14.i3.pp1382-1393
13. Firouzi, M. (2018). A modified capacitive bridge-type fault current limiter (CBFCL) for LVRT performance enhancement of wind power plants. *International Transactions on Electrical Energy Systems, 28(3),* 1-15. https://doi.org/10.1002/2050-7038.12418
14. Golshannavaz, S., Aminifar, F., & Nazarpour, D. (2014). Application of UPFC to Enhancing Oscillatory Response of Series-Compensated Wind Farm Integrations. *IEEE Transactions on Smart Grid, 5(4),* 1961-1968. https://doi.org/10.1109/TSG.2013.2294424
15. Guoyi, X., Lie, X., & Morrow, J. (2013). Power oscillation damping using wind turbines with energy storage systems. *IET Renewable Power Generation, 7(5),* 449–457. https://doi.org/10.1049/iet-rpg.2012.0231
16. Hosseini, E., Behzadfar, N., Hashemi, M., Moazzami, M., & Dehghani, M. (2022). Control of Pitch Angle in Wind Turbine Based on Doubly Fed Induction Generator Using Fuzzy Logic Method. *Journal of Renewable Energy and Environment, 9(2),* 1-7. https://doi.org/10.30501/jree.2021.293546.1226
17. Huang, C., Xiao, X. Y., Zheng, Z., & Wang, Y. (2019). Cooperative Control of SFCL and SMES for Protecting PMSG-Based WTGs Under Grid Faults. *IEEE Transactions on Applied Superconductivity, 29(2),* 1-6. https://doi.org/10.1109/TASC.2018.2872358
18. Inoue, Y., Morimoto, S., & Sanada, M. (2008). Output maximization using direct torque control for sensorless variable wind generation system employing IPMSG. *In Proceedings of the 13th International Power Electronics and Motion Control Conference* (pp.1859-1865). https://doi.org/10.1109/EPEPEMC.2008.4635767
19. Ji, T., He, X., Li, X., Liu, K., & Zhang, M. (2014). Performance analysis and research on LVRT of PMSG wind power systems with SDBR. *In Proceedings of the 33rd Chinese Control Conference* (pp.6953–6958). https://doi.org/10.1109/ChiCC.2014.6896146
20. Kim, K., Jeung, Y., Lee, D., & Kim, H. (2012). LVRT Scheme of PMSG Wind Power Systems Based on Feedback Linearization. *IEEE Transactions on Power Electronics, 27(5),* 2376-2384. https://doi.org/10.1109/TPEL.2011.2172160
21. Kwon, J. M., Kim, J. H., Kwak, S. H., & Lee, H. H. (2008). Optimal power extraction algorithm for DTC in wind power generation systems. *IEEE International Conference on Sustainable Energy Technologies* (pp. 639-643). https://doi.org/10.1109/ICSET.2008.4745479
22. Laghridat, H., Essadki, A., & Nasser, T. (2022). Coordinated control by ADRC strategy for a wind farm based on SCIG considering low voltage ride-through capability. *Protection and Control of Modern Power Systems, 7(7),* 1-11. https://doi.org/10.1186/s41601-022-00298-3
23. Liu, M. et al. (2023). ADRC-based optimized control system for wind turbine power generator. *Advanced Control for Applications: Engineering and Industrial Systems*. https://doi.org/10.1002/adc2.142
24. Lu, M. S., Chang, C. L., Lee, W. J., & Wang, L. (2009). Combining the wind power generation system with energy

storage equipments. *IEEE Transactions on Industry Applications, 45(6)*, 2109-2115. https://doi.org/10.1109/08IAS.2008.139

25. Merabet, A., Ahmed, K. T., Ibrahim, H., & Beguenane, R. (2016). Implementation of Sliding Mode Control System for Generator and Grid Sides Control of Wind Energy Conversion System. *IEEE Transactions on Sustainable Energy, 7(3)*, 1327-1335. https://doi.org/10.1109/TSTE.2015.2510041
26. Mohod, S. W., & Aware, M. V. (2010). A STATCOM-Control Scheme for Grid Connected wind Energy System for Power Quality Improvement. *IEEE Systems Journal, 4(3)*, 346-352. https://doi.org/10.1109/JSYST.2010.2050972
27. Muyeen, S. M., & Al-Durra, A. (2013). Modeling and Control Strategies of Fuzzy Logic Controlled Inverter System for Grid Interconnected Variable Speed Wind Generator. *IEEE Systems Journal, 7(4)*, 817-824. https://doi.org/10.1109/JSYST.2013.2270416
28. Nguyen, T. H., & Lee, D. (2013). Advanced Fault Ride-Through Technique for PMSG Wind Turbine Systems Using Line-Side Converter as STATCOM. *IEEE Transactions on Industrial Electronics, 60(7)*, 2842-2850. https://doi.org/10.1109/TIE.2012.2211539
29. Nguyen, T. H., & Lee, D. C. (2010). Ride-through technique for PMSG wind turbines using energy storage systems. *Journal of Power Electronics, 10(6)*, 733–738. https://doi.org/10.6113/JPE.2010.10.6.733
30. Pannell, G., Zahawi, B., Atkinson, D. J., & Missailidis, P. (2013). Evaluation of the Performance of a DC-Link Brake Chopper as a DFIG Low-Voltage Fault-Ride-Through Device. *IEEE Transactions on Energy Conversion, 28(3)*, 535-542. https://doi.org/10.1109/TEC.2013.2254763
31. Penne, M., Qiao, W., Qu, L., Huang, R., & Huang, Q. (2021). Active Disturbance Rejection Control of Doubly-Fed Induction Generators Driven by Wind Turbines. *In 2021 IEEE Energy Conversion Congress and Exposition (ECCE)* (pp. 965-972). Vancouver, BC, Canada. https://doi.org/10.1109/ECCE47101.2021.9595083.
32. Rahim, A. H. M. A., & Nowicki, E. P. (2012). Supercapacitor energy storage system for fault ride-through of a DFIG wind generation system. *Energy Conversion and Management, 59*, 96–102. https://doi.org/10.1016/j.enconman.2011.12.023
33. Ramirez, D., Martinez, S., Platero, C. A., Blazquez, F., & de Castro, R. M. (2011). Low-Voltage Ride-Through Capability for Wind Generators Based on Dynamic Voltage Restorers. *IEEE Transactions on Energy Conversion, 26(1)*, 195-203. https://doi.org/10.1109/TEC.2010.2096049
34. Raphael, S., & Massoud, A. (2011). Unified power flow controller for low voltage ride through capability of wind-based renewable energy grid-connected systems. *Eighth International Multi-Conference on Systems, Signals & Devices*,1-6. http://dx.doi.org/10.1109/SSD.2011.5767399
35. Shi, J., Tang, Y., Xia, Y., Ren, L., & Li, J. (2011). SMES Based Excitation System for Doubly-Fed Induction Generator in Wind Power Application. *IEEE Transactions on Applied Superconductivity, 21(3)*, 1105-1108. https://doi.org/10.1109/TASC.2010.2090584
36. Soliman, M. A., Hasanien, H. M., Azazi, H. Z., El-Kholy, E. E., & Mahmoud, S. A. (2019). An Adaptive Fuzzy Logic Control Strategy for Performance Enhancement of a Grid-Connected PMSG-Based Wind Turbine. *IEEE Transactions on Industrial Informatics, 15(6)*, 3163-3173. https://doi.org/10.1109/TII.2019.2910329
37. Thet, A. K., & Saitoh, H. (2009). Pitch control for improving the low-voltage ride-through of wind farm. *In Proceedings of Transmission and Distribution Conference and Exhibition, Asia Pacific* (pp. 1-4). https://doi.org/10.1109/TDC-ASIA.2009.5357459
38. Valenciaga, F., & Puleston, P. F. (2008). High-Order Sliding Control for a Wind Energy Conversion System Based on a Permanent Magnet Synchronous Generator. *IEEE Transactions on Energy Conversion, 23(3)*, 860-867. https://doi.org/10.1109/TEC.2008.926750
39. Yaramasu, V., Wu, B., Alepuz, S., & Kouro, S. (2014). Predictive Control for Low-Voltage Ride-Through Enhancement of Three-Level-Boost and NPC-Converter-Based PMSG Wind Turbine. *IEEE Transactions on Industrial Electronics, 61(12)*, 6832-6843. https://doi.org/10.1109/TIE.2013.2295785
40. Yehia, D. M., Mansour, D. A., & Yuan, W. (2018). Fault Ride-Through Enhancement of PMSG Wind Turbines With DC Microgrids Using Resistive-Type SFCL. *IEEE Transactions on Applied Superconductivity, 28(4)*, 1-5. https://doi.org/10.1109/TASC.2017.2769400
41. Wang, L., & Truong, D. N. (2012). Dynamic Stability Improvement of Four Parallel-Operated PMSG-Based Offshore Wind Turbine Generators Fed to a Power System Using STATCOM. *IEEE Transactions on Power Delivery, 28(1)*, 111-119. https://doi.org/10.1109/TPWRD.2012.2219441
42. Wang, Z., Fan, J., Meng, Y., Sun, Z., Zhou, Z., & Cui, J. (2023). Active Disturbance Rejection Control Strategy for Permanent Magnet Synchronous Wind Power System. *In 2023 8th Asia Conference on Power and Electrical Engineering (ACPEE)* (pp. 811-815). Tianjin, China. https://doi.org/10.1109/ACPEE56931.2023.10135913.